Published in final edited form as:
Neuroimage. 2014 November 1; 101: 21–34. doi:10.1016/j.neuroimage.2014.06.038.

SimPACE: generating simulated motion corrupted BOLD data with synthetic-navigated acquisition for the development and evaluation of SLOMOCO: a new, highly effective slicewise motion correction

Erik B. Beall[a,*] and **Mark J. Lowe**[a]

[a]Imaging Institute, Cleveland Clinic, 9500 Euclid Ave., Cleveland, OH 44195, USA

Abstract

Head motion in functional MRI and resting-state MRI is a major problem. Existing methods do not robustly reflect the true level of motion artifact for in vivo fMRI data. The primary issue is that current methods assume motion is synchronized to the volume acquisition and thus ignore intra-volume motion. This manuscript covers three sections in the use of gold-standard motion-corrupted data to pursue an intra-volume motion correction. First, we present a way to get motion corrupted data with accurately known motion at the slice acquisition level. This technique simulates important data acquisition-related motion artifacts while acquiring real BOLD MRI data. It is based on a novel motion-injection pulse sequence that introduces known motion independently for every slice: Simulated Prospective Acquisition CorrEction (SimPACE). Secondly, with data acquired using SimPACE, we evaluate several motion correction and characterization techniques, including several commonly used BOLD signal- and motion parameter-based metrics. Finally, we introduce and evaluate a novel, slice-based motion correction technique. Our novel method, SLice-Oriented MOtion COrrection (SLOMOCO) performs better than the volumetric methods and, moreover, accurately detects the motion of independent slices, in this case equivalent to the known injected motion. We demonstrate that SLOMOCO can model and correct for nearly all effects of motion in BOLD data. Also, none of the commonly used motion metrics was observed to robustly identify motion corrupted events, especially in the most realistic scenario of sudden head movement. For some popular metrics, performance was poor even when using the ideal known slice motion instead of volumetric parameters. This has negative implications for methods relying on these metrics, such as recently proposed motion correction methods such as data censoring and global signal regression.

*Address for correspondence and reprints: Erik B. Beall, PhD, Cleveland Clinic, 9500 Euclid Ave, U-15, Cleveland, OH 44195, Phone: 216-445-6110, Fax: 216-636-2397, ebeall@gmail.com.

Keywords

functional MRI; functional connectivity; BOLD; motion correction; spin history

Introduction

Head motion is largely considered an intractable problem in functional MRI (fMRI) and resting-state fMRI (RS-fMRI). Nearly all fMRI studies rely on blood oxygenation level-dependent (BOLD) contrast, generated by a vascular response to increased neuronal activity. BOLD signal changes, whether spontaneous or in response to a stimulus, are relatively small, at most a few percent of the average signal level. Therefore, head motion during acquisition can result in signal changes from several underlying processes that can easily be greater than the BOLD signal changes, reducing sensitivity and specificity (Bullmore et al., 1999; Friston et al., 1995; Friston et al., 1996; Hajnal et al., 1994; Hajnal et al., 1995). Subtle differences in motion characteristics can affect the conclusions drawn by a study (Bullmore et al., 1999; Lund et al., 2005) and important past findings have been called into question by recent work (Hallquist et al., 2013; Power et al.,; Satterthwaite et al.,; Van Dijk et al.).

There are many motion correction strategies at present, but these are limited by the assumption that motion is synchronized to the volume acquisition[1]. To test the sensitivity to intra-volume motion and develop an intra-volume correction, new methods are needed. The first requirement is realistic BOLD-weighted validation data with known intra-volume motion corruption in order to assess volumetric and intra-volume methods. This is important because past validations have been limited to evaluating the effects on variance reduction in live human data, the effects on residuals in simple partial volume simulated data, or the average activation in real data(Ardekani et al., 2001; Morgan et al., 2007; Morgan et al., 2001; Oakes et al., 2005; Wu et al., 1997; Xu et al., 2007) (Johnstone et al., 2006). These evaluations all used either real data with unknown motion, neuronal and physiologic activity or simulations that did not model motion effects realistically. Therefore, we first require realistic BOLD data with known intravolume motion.

Realistic Intra-Volume Motion Corrupted Data

BOLD MRI is, in the vast majority of cases, acquired with 2D echoplanar imaging (EPI), and in EPI individual slices are acquired separately in time on a temporal grid spaced over the volumetric repetition time (TR). Newer multiband EPI is similar, except that two or more spatially-separated slices are acquired simultaneously. Most current motion correction techniques assume that when motion occurs, the entire volume is affected the same way. The volumetric, partial-volume effects are hence termed the first-order motion effects. This assumption reduces the problem of correcting the motion to a simple head registration problem. Volumetric motion registration methods determine the average head motion over a

[1]There is a method to interpolate volumetric motion to the slice acquisition Roche, A., 2011. A four-dimensional registration algorithm with application to joint correction of motion and slice timing in fMRI. IEEE Trans Med Imaging 30, 1546-1554., but the resulting motion at each slice remains a function of the volume motion.

volume, and this average volume-to-volume motion can be removed using either a prospective motion correction during data acquisition(Thesen et al., 2000) or a retrospective motion correction after acquisition(Cox and Jesmanowicz, 1999; Friston et al., 1995; Hajnal et al., 1995; Jenkinson et al., 2002; Jiang et al., 1995). Most importantly, these methods do not remove the intra-volume out-of-plane motion artifact or other second-order effects. Second-order motion artifacts arise from four primary sources: spin history, intra-volume partial-volume, B1 inhomogeneity, and B0 inhomogeneity. Spin history effects can dominate the acquisition and are solely due to out-of-plane motion(Friston et al., 1996; Muresan et al., 2005). These effects are discussed in more detail in the supplement.

We implemented a simple experimental method that acquires a BOLD-weighted MRI dataset with an “inverted” prospective motion correction. By altering the gradient axes on-the-fly independently for each slice according to pre-defined motion parameters, we can inject arbitrary motion with very high accuracy: Simulated Prospective Acquisition CorrEction (SimPACE), described in more detail in **Theory**. Note that this sequence does not simulate intra-slice motion, and any data it produces must assume that motion occurs exactly at the slice raster, which is not entirely realistic. Note also that this sequence cannot produce B0 shim change effects or B1 receive/transmit field effects, but it will obtain most of the signal changes due to real head motion, including intra-volume partial volume, spin history and B0 phase-encode image warping effects. This simple modification allows the creation of real BOLD data with accurately-reproduced signal artifacts. Acquisition of such data in cadavers and live subjects represents gold-standard data that can be used to test existing motion characterization and correction methods with a ground truth. In this study, we acquired gold-standard known-motion BOLD data in living subjects at rest and in cadavers using this sequence.

Motion Correction Methods

Motion correction methods used in BOLD MRI are well known to fMRI researchers. Nearly all head motion correction strategies include a method to detect the correct sampling grid using the data and then resample accordingly at the boundaries of each volume acquisition. In most implementations, head motion is assumed to be rigid-body motion, with 3 translations and 3 rotations comprising the 6 degrees of freedom (DOF) of rigid-body motion. Volumetric correction for BOLD MRI was initially done in the early days of fMRI by adapting Roger Woods’ automated image registration (AIR) algorithm, originally developed for PET functional imaging studies(Woods et al., 1992). BOLD-specific methods, which were initially described nearly 20 years ago(Friston et al., 1995; Hajnal et al., 1994; Hajnal et al., 1995), have since undergone rapid development(Ardekani et al., 2001; Cox and Jesmanowicz, 1999; Derbyshire et al., 1998; Lee et al., 1998; Thesen et al., 2000), and have been implemented comparably(Ardekani et al., 2001; Morgan et al., 2007; Morgan et al., 2001; Oakes et al., 2005) across common MRI analysis packages(Cox, 1996; http://www.fil.ion.ucl.ac.uk/spm, ; Smith et al., 2004). These methods all rely on using small displacement approximations to produce an analytic solution (unlike the AIR method, which is an iterative, generalized method). These techniques resample the volume to be corrected and compare the repeatedly updated resampled volume to a “base” image using a search for the minimum total difference through various cost functions. Robustness is dependent on

signal-to-noise ratio (SNR), image contrast, the assumption of small, volumetric head motion (or continuous smoothly interpolated motion(Roche, 2011)), and sufficient image coverage in 3 dimensions.

Residual effects of motion that remain in the corrected data are typically modeled retrospectively using the motion parameters from the motion correction. In this method, a second-order polynomial function of the motion parameters or a Taylor series expansion of the effect on the Bloch equations (and possibly containing derivatives of these) can be least-squares fitted to the timeseries data(Bullmore et al., 1999; Friston et al., 1996). The regressed model is subsequently subtracted to attenuate the motion artifact, which we call *second-order motion correction*. Early work demonstrated efficacy using the volumetric parameters(Friston et al., 1996), but later work extended this to the more appropriate trigonometrically-derived voxelspecific displacements based on the volumetric parameters(Bullmore et al., 1999). This method can be useful in attenuating severe motion artifact associated with difficult patient populations such as those with movement disorders(Beall et al., 2013), but unavoidable overlap with the experimental paradigm or BOLD signal results in a reduction in sensitivity for fMRI studies. As the complexity of the model is increased in an attempt to model more of the motion-related artifact, BOLD sensitivity drops. This is true regardless of what is being regressed, including arbitrary random vectors, and the only way to reduce this loss is to reduce the number of regressors(Beall, 2010).

Motion Characterization

The characterization of motion present in data is almost as important as motion correction. For many years, the most reliable way to assess for motion present in data was a qualitative “visual inspection” of the resulting statistical map by an experienced researcher. This, of course, is very subjective and is only relatively robust for the assessment of false positive increase from stimulus-correlated motion in block-style fMRI paradigm designs. An increase in false negatives is difficult to assess visually since it cannot be distinguished from reduced connectivity or activation, such as is the case for event-related fMRI, connectivity and block fMRI with stimulus-uncorrelated motion. Many objective, quantitative motion metrics have been proposed over the years, the first being that of Jiang et al. (Jiang et al., 1995). They proposed to use the average voxel displacement over the voxels intersecting a parallelipiped running in the dorso-ventral direction centered on the isocenter of the volume, or total displacement (TD). The dominant practice in the field at present relies on simpler metrics based on the vector sum of the effect of all 6 DOF motion parameters on a voxel at the edge of the brain(Jenkinson et al., 2002; Power et al., 2011). The first derivative of motion parameters or the RMS difference between subsequent motion matrices(Jenkinson et al., 2002) is computed. Then each rotation is converted to representative edge-of-brain translation by multiplying the rotation by a value approximating the radius of the human head. The vector sum across the first derivative volume translations and these converted rotational translations produces a single metric for each volume. Metrics such as these are used for quality control, in censoring methods or, in the case of the global BOLD signal, as a regressor of no interest that is intended to capture variance due to motion and physiology. In this study, the accuracy of each metric at capturing motion-related variance is examined

using SimPACE data. A detailed discussion of motion censoring and global signal regression as motion correction is included in the supplemental material.

Intra-Volume Motion Correction

The results of our investigations with SimPACE cadaver data led us to believe an intra-volume correction was possible. A key finding was the realization that the volumetric parameters are related to the sum of the slice motion. This insight led us to the development of an algorithm to estimate the out-of-plane motion and correct the data using these estimates: SLice-Oriented MOtion COrrection (SLOMOCO). Our method is not a coregistration technique, but a slicewise rigid-body motion parameter estimation and subsequent correction through regression using these parameters. We will show that, with our implementation, we observe motion estimates that correspond to the true motion. We will also show that with our algorithm the correspondence is stable over time. Thus, these motion estimates can be used as regressors in a voxel- and slice-accurate motion model. First, we perform an in-plane slicewise (intra-volume) motion correction. Then, we freeze the motion on all slices but a slice of interest and pass the mostly frozen volume to a standard volumetric correction. This is repeated for all slices. Finally, we use these motion estimates in a voxel- *and slice*-specific second-order motion regression. If these motion estimates correlate very highly with the true motion, then they will be suitable for regression, regardless of the correctness of the amplitude of the motion estimates. We show with SimPACE and in real data, that this is indeed the case and that the estimated motion parameters correlate very highly with the true motion parameters.

Our objective in this study was to use a new acquisition, SimPACE, to test, evaluate and develop motion methods. For motion characterization, we evaluate the efficacy of several metrics based on volumetric motion parameters and metrics based on BOLD signals that have been used in the literature and demonstrate that none of them are effective at robustly identifying realistic motion corrupted volumes in fMRI data. For motion correction, we compare the accuracy of 3 widely-used volumetric correction methods and we compare the effect on motionrelated signal from second-order correction (volumetric and voxel-specific). Finally, we compare SLOMOCO and show that this technique produces a correction that is superior to existing methods.

Materials and Methods

Study overview

In this study, we acquired BOLD-weighted data obtained with a motion-injection pulse sequence (described in the Appendix: SimPACE) in cadavers and living subjects and compared the true motion with the efficacy of several motion characterization metrics. We then compared the efficacy of several motion correction methods, including SLOMOCO. To assess the effect of each method on motion-related signal, we compared the image standard deviation in cadaver data across corrections described in detail in the Appendix.

Study population

This study made use of cadaver data acquired through a rapid postmortem protocol study described in Fisher et al(Fisher et al., 2007). MRI data were acquired from a total of 7 cadaver subjects (all cadavers scanned within 8 hours postmortem and before any tissue removal). The collection and use of human tissue were approved by Cleveland Clinic's Institutional Review Board. A total of 2 male and 1 female live healthy participants (mean age, 35 y; range, 33–38 y) were recruited for MRI examination (controls). All study procedures were approved by the Cleveland Clinic's Institutional Review Board, and all research participants provided informed consent after receiving complete verbal and written descriptions of the study.

MRI data acquisition

Two scans were acquired in all subjects. Data were acquired with a 12-channel receiveonly head array on a Siemens Trio 3T scanner (Siemens Medical Solutions, Erlangen, Germany). All controls were fitted for a bite bar to restrict head motion during scanning. Each scan session consisted of the following scans:

- **Scan 1:** Anatomic 3D whole-brain T1 study: T1-weighted inversion recovery turboflash (MPRAGE); 176 axial slices; thickness, 1 mm; field of view, 256 mm × 256 mm; TR/echo time/inversion time/flip angle, 1900 ms/1.71 ms/900 ms/8°.
- **Scan 2:** Resting connectivity scan (rest): Whole-brain BOLD-weighted EPI sequence using SimPACE and a motion injection vector file described in the supplementary material. 132 repetitions of 31-4 mm thick axial slices; echo time/TR, 29 ms/2,800 ms; matrix, 128 × 128; field of view, 256 mm × 256 mm; receive bandwidth, 250 kHz. Controls were instructed to rest with their eyes closed and refrain from any voluntary motion.

For controls, physiologic signals were acquired with a pulse oximeter on the index finger of the left hand and with respiratory bellows around the chest in Scan 2. Physiologic timing files were synchronized to scanner data acquisition according to a previously published method (Beall and Lowe, 2007).

Image postprocessing

The functional connectivity MRI data from Scan 2 were branched into multiple parallel correction pipelines. A comparison of three commonly used volumetric corrections is described in the supplement. For simplicity of presentation, we present results here using 3dvolreg from AFNI. After volumetric head motion correction with AFNI (Cox, 1996), the data were branched down two separate pipelines to compare second-order motion correction methods including $\mathbf{S}^{\mathbf{VOL}}$ (Friston et al., 1996) as described in Eqn 2 and $\mathbf{S}^{\mathbf{VOX}}$ (Bullmore et al., 1999) as described in Eqn 3 (see Appendix for equations and details). Briefly, second-order motion correction methods are regression-based corrections that consist of fitting and then removing the projection of various motion models at every voxel. The primary difference between these models is the use of either the same motion model matrix for all voxels as in $\mathbf{S}^{\mathbf{VOL}}$ or a unique, trigonometrically-derived motion model matrix for each voxel, as in $\mathbf{S}^{\mathbf{VOX}}$. These corrections were performed using volumetric motion parameters to

construct the motion models. This study also sought to compare effectiveness of slicewise motion parameters. Thus, for additional comparisons using the known, true injected slicewise motion and SLOMOCO-detected slicewise motion, we branched the data down two additional separate pipelines both using $\mathbf{S}^{\mathbf{VOX\text{-}SLC}}$ as described in Eqns 5 & 6; one corrected using the injected slicewise parameters and the other corrected using SLOMOCO. For data corrected with $\mathbf{S}^{\mathbf{VOX\text{-}SLC}}$ no volumetric correction was performed first. Additional comparisons are included in the supplement, using the other models and a volume-averaged form of the true injected slicewise motion. No further corrections were performed.

A separate pipeline correction was performed to demonstrate the effect of $\mathbf{S}^{\mathbf{VOL}}$, $\mathbf{S}^{\mathbf{VOX}}$ and $\mathbf{S}^{\mathbf{VOX\text{-}SLC}}$ on false positives due to motion in functional connectivity MRI data. In this pipeline, the data for controls were corrected for volumetric motion and were then corrected for adaptive physiologic noise sources using the monitored physiologic data and the PESTICA for AFNI v2.0(Beall, 2010; Beall and Lowe, 2007); the three variations of second-order motion correction were then performed as described above. Cadaver data were corrected in the same way but without physiologic correction. Corrected data were then spatially filtered and analyzed using tools integrated with InstaCorr from AFNI(Jo et al.), and connectivity maps were generated for the posterior cingulate and left primary motor cortex. The purpose of this final comparison is to demonstrate the use of these three corrections in real data and show there is a visible effect on false positive rate. We stress that it is not possible to separate the false positive and false negative voxels from such a simple analysis.

Data Analysis

Image motion metric analysis and global signal

BOLD-based motion metrics: Four variants of average BOLD signal were computed: 1) global signal (GS), 2) percent global signal (PGS), 3) global root-mean-square (RMS) signal (VARS), and 4) DVARS(Power et al., 2011). GS was computed by averaging the signal at each voxel over the entire brain; the result was then detrended to obtain the GS. Following this step, the mean signal level of every voxel was normalized to 1000 and only voxels completely inside the brain at all timepoints were used, as described in Power et al(Power et al., 2011). PGS was computed by first subtracting the mean over time, detrending and then dividing by the mean (over time) signal at each voxel, and then taking the average over the entire brain. VARS was computed by calculating the square of the detrended and de-meaned image data before summation over voxels and then calculating the square root of the resulting timeseries. The VARS metric was so named for consistency with the DVARS metric, as it is the same measure but created without taking the first derivative. The DVARS (or 1^{st} temporal derivative of the RMS signal)(Power et al., 2011) was computed by first subtracting the previous timepoint from each timepoint of the detrended data to generate a new difference timeseries, which was then squared, summed over voxels and the square root of the resulting timeseries was taken. A threshold of 0.5 DVARS was used to identify corrupted volumes(Power et al., 2011), and this was the threshold used for all BOLD signal-based metrics.

Volumetric motion metrics: The volumetric motion parameters from each volumetric correction were converted into several motion metrics. However, it is important to note that there are currently two different ways of using the motion parameters: absolute and relative motion. Absolute motion means simply taking the motion metrics without any further processing, while relative motion means taking the difference between subsequent volumes. The relative motion will be referred to herein with the suffix -1D, because it is created by taking the difference between subsequent volumes, or the first derivative. The absolute motion will be referred to with the suffix -0D, because there is no derivative taken. We make no claims here as to which is more appropriate (beyond showing that neither works well), but note that both are commonly used, with first derivative being more popular. These -0D or -1D parameters are then used to generate various motion metrics.

The metrics included 1) the method of *Jiang et al* for mean *voxelwise* total displacement (TD) over a parallelepiped centered on isocenter of the acquired volume(Jiang et al., 1995); 2) the square root of the sum of squares of the *volumetric* translations (VTD)(Van Dijk et al., 2012); and 3) framewise displacement (FD) or the straight sum across the 6 absolute value *volumetric* motion parameters, after first converting rotations to displacements on a 50mm sphere(Power et al., 2011). Thus we generated the following motion metrics for each dataset: TD-1D, TD-0D, VTD-1D, VTD-0D, FD-1D and FD-0D. For identification of corrupted volumes, a threshold of 0.5 was used for TD and FD(Power et al., 2011) and a threshold of 0.1 was used for VTD(Van Dijk et al., 2012), both 0D and 1D forms.

Slicewise motion metrics: Additionally, each of these measures was computed using the slicewise injected motion parameters (TRU): TD-1D-TRU, TD-0D-TRU, VTD-1D-TRU, VTD-0D-TRU, FD-1D-TRU and FD-0D-TRU. These all have the suffix –TRU added to indicate that these are a version of the metric calculated using the true motion. The TRU motion metrics contain more datapoints (the number of slices times volumes) than the other metrics, so for comparison, each TRU metric was converted to a volumetric form. Because the intent is to identify volumes containing motion corruption, the metric should be sensitive to the largest motion within a volume. Therefore, the maximum slicewise motion within each volume was taken and used as the motion for that volume. This is denoted by the additional suffix –TRU– SLC.

To evaluate the correspondence between these metrics, each metric was used to identify motion corruption using thresholds as described in published reports. The indices corresponding to known motion corruption events were compared to indices detected by each metric. Finally, the various motion metrics and global signals were plotted for visual inspection, to demonstrate the relative robustness of identification of motion corrupted volumes associated with each metric and illustrate differences in sensitivity to motion that is primarily rotational or translational.

Volumetric correction performance analysis: correlation and NMSE with ground truth—To compare the true injected motion parameters with the detected volumetric parameters, the injection vectors must be averaged across the volume to produce a single set of rigid-body parameters per volume. In contrast to the process described above for the TRU–SLC metrics, in this case it is the average motion that is most relevant to

detected volumetric parameters. Therefore, for each volume of the injected motion parameters the average was taken over the slices, separately for each of the 6 DOFs. This is denoted by the additional suffix –TRU–VOL. The volumetric motion parameters obtained were then compared with the TRU–VOL injected motion parameters using Pearson linear correlation. Results for each of 3 different software tools are given in the tables, with more details in the Supplement. The distribution of motion parameters was assessed for significantly different means between tools using a 2-sample t-test and a corrected *p*-value of 0.05. The Pearson linear correlation is not sensitive to amplitude, so we examined how closely the detected motion amplitude followed the injected motion using the normalized mean square error (NMSE). In the following calculations NMSE is the ratio of the standard deviation of the difference to the standard deviation of the average motion, as described in Eqn 1, where ×= (detected motion – injected motion) and y = ½ (detected motion + injected motion).

$$NMSE = \sqrt{\frac{\sum_{i=1}^{N}(x_i - \bar{x})^2}{\sum_{i-1}^{N}(y_i - \bar{y})^2}} \quad \text{Eqn1}$$

Motion correction comparison: image temporal variance—The temporal standard deviation (tSTD) of the raw data and each motion corrected dataset was computed within a whole-brain mask and a histogram was created. The mean brain tSTD was computed for each dataset's histogram and stored. The mean and standard deviation of this mean tSTD across subjects was computed and reported.

Results

Image motion metric analysis and global signal

Table 1 shows the percent of timepoints during realistic motion-injection identified as corrupted with each volumetric metric, the percent of timepoints that correctly corresponded to injected motion timepoints and the percent of timepoints misidentified as motion. The table shows that DVARS and VARS metrics identified no volumes as corrupted at the 0.5 threshold, and slightly better performance at a lower threshold of 0.1. Note it is possible that FD and TD may perform better if different thresholds were used, we simply used the thresholds from the literature(Power et al., 2011; Van Dijk et al., 2012). In the lower section of Table 1, the metrics based on slicewise injected motion (TRU) are also shown for comparison. Note these are idealized metrics, because the slicewise true motion is not available in standard practice, thus these are intended only to show that with slicewise motion, one can identify corruption events with high accuracy and specificity, in comparison with those metrics based on volumetric parameters, which do not perform well.

Figures 3 and 4 show motion metrics derived on two distinct segments of SimPACE data. Figure 3 shows metrics during realistic (intra-volume) motion injection and Figure 4 shows metrics during unrealistic (volumetric) motion injection. Figures 3a and 4a shows the four mean signal metrics: GS, PGS, VARS and DVARS. Figures 3b and 4b shows 1D volumetric

(AFNI) motion parameter-based motion metrics (TD-1D, FD-1D and VTD-1D) with the 0D form of TD based on the original injected motion parameters at every slice (TD-0D-TRU). Figures 3c and 4c shows the non-derivative motion parameter-based motion metrics (TD-0D, FD-0D and VTD-0D). These metrics produce very different results and, of note, the 1D-based mean BOLD signal (DVARS) indicates that for every moderate to large motion injected, there are two adjacent volumes that would be indicated as being equally corrupted (see Figure 5, all peaks of derivative-based metrics are 2 volumes wide). However, this is not the case, as the signal artifact in individual voxels is predominantly synchronous with the instantaneously injected motion. This clearly presents a problem for all 1D-based metrics, whether based on signal changes or motion parameters. Figures 3 and 4 demonstrate that in-plane (3DOF) translation parameter-based metrics (VTD-0D and VTD-1D) have dramatically different sensitivity to rotational and translational motion. Figure 4 has notations indicating rotational motion injection, demonstrating that VTD is not as sensitive as the other measures to rotational motion. Further, motion occurring on only a few slices, during the slices-only injection phase of the scan, is not detected well by either signal-based or parameter-based methods. Figure 3 shows clearly that volumetric motion parameter-derived metrics miss non-volumetric motion. This inaccuracy is proportional to the number of slices with a given motion, and thus in real data, volumetric-based motion parameters miss on average *at least 50% of the motion*. Multiple independent directions of motion within a given volume may actually increase the amount of missed motion.

Volumetric correction performance analysis: correlation and NMSE with ground truth

The motion parameters obtained from all software tools were highly accurate when compared to the volume-averaged injected TRU motion. These findings were true both for linear correlation and NMSE measures. It is important to note that in order to make comparisons among different software, the parameters must be converted to have the same rotational origin. FSL rotation is about the corner of the image cube, rather than image center, so for comparison, these were converted to center of image following the MATLAB code detailed in the Supplement.

For SLOMOCO detected motion parameters, the linear correlation to the injected motion was very high (Table 4). A slicewise examination of accuracy showed that slices at the outer edges of the volume had poor correlation to injected motion, while all other slices had a very strong correlation with the injected motion (Figure 7). If one discards the outermost slices, the performance of this method is excellent.

Motion correction comparison: image temporal variance

As can be seen in the cadaver data columns of Table 5, the image noise is reduced by over half (56% reduction in tSTD) by the best corrections (second-order correction using the retrospective SLOMOCO method). Volumetric coregistration alone (VOL in Table 5) performed about half as well by comparison, reducing image standard deviation by 27%. Second-order correction with the volumetric model produced a modest improvement of a further 13% (S^{VOL} and VOL+S^{VOL}), marking a further improvement of about halfway to the best corrections. Meanwhile, the voxel-specific model, using the retrospective motion parameters (S^{VOX} in Table 5) performed nearly as well as the fully slicewise model

($S^{VOX-SLC}$ with SLOMOCO). Additional data from previously-acquired cadaver brains was examined for a baseline measurement of tSTD without motion injection. This data was identical to the SimPACE data except for the lack of injected motion, and shows the level of non-motion noise present in this data. The cadaver baseline data indicates that common motion correction methods can account for between 52 and 74% of the motion-related artifact.

Table 6 shows the same, but using the injected truth motion as the basis for each motion correction. Interestingly, the use of volume-averaged truth motion in regression models produced very similar reduction in tSTD as when using the retrospective motion parameters. The best performance came when using slice-wise motion, whether using retrospective slicewise motion ($S^{VOX-SLC}$ SLOMOCO in Table 5) or the truth slicewise motion ($S^{VOX-SLC}$ TRU-SLC in Table 6). The voxel-specific volumetric model (S^{VOX} in Table 5 or S^{VOX} TRU-AVG or TRU-SLC in Table 6) approached this performance but the fully slicewise models performed better by about five percent. It is interesting to note that in live subjects, the fully retrospective models (Table 5, last column) performed better than truth. We believe this may be due to small real subject motion in these live subjects that caused the actual motion to deviate from the TRU motion parameters. In live subjects, there will be some real unanticipated motion such that TRU motion parameters deviate from the actual motion. In cadaver data, there is no such deviation and TRU motion is the actual motion, which was the primary motivation for obtaining the cadaver data.

Figure 7 shows seeded connectivity maps in a cadaver and Figure 8 in live subject SimPACE data corrected with VOL, VOL+ S^{VOL}, VOL+ S^{VOX}, using $S^{VOX-SLC}$ with SLOMOCO and $S^{VOX-SLC}$ with TRU parameters prior to spatial filtering and analysis, demonstrating a reduction of motion artifact that was not removed by the current best methods available (S^{VOL} or S^{VOX}). In the case of the cadaver data, SLOMOCO correction was comparable to TRU, while in live subject data SLOMOCO performed better than TRU, presumably because of real additional subject motion such that the true motion deviated from TRU. Insets in the lower right of each figure show a representative voxel timecourse after each correction (see Supplement for additional displays).

In a supplementary analysis, we simulated the effect of BOLD contamination on estimated motion from SLOMOCO. This is described in the supplement, but we note here we did not observe a change in the SLOMOCO estimates from the presence of BOLD signal contamination.

Discussion

We have demonstrated that motion injection with SimPACE is useful for the evaluation of motion correction methods. Using cadaver data acquired with SimPACE, we have demonstrated that commonly used motion metrics based on volumetric motion estimation are not robust estimators of actual motion. We have further shown with SimPACE that for BOLD-weighted data, if one knows the motion parameters for every slice, it is possible to remove most of the motion artifact. Finally, we have demonstrated the effectiveness of a new, retrospective algorithm that obtains accurate motion parameters for nearly all slices

and provides an avenue for retrospective correction of motion-corrupted BOLD-weighted MRI data.

As assessed with correlation and mean square difference, SPM, AFNI and FSL performed equally well at obtaining the correct motion parameters. However, it is important to note that while AFNI and SPM assume the image center for rotations, FSL's mcflirt (v5.0.2) is instead converted to rotations about the first image voxel in the lower image corner. The result is that the translation parameters reported (MAT files) by mcflirt (v5.02) must be converted prior to comparison with other tools. Furthermore, all versions of the motion metrics compared herein may be inappropriate if this is not accounted for. In particular, FSL-derived TD and FD may count the effect of rotations about center of mass more strongly, and in a manner dependent on the image field of view because the translations will include center of mass rotation multiplied by the distance to image corner (for small angles). This issue could also negatively affect second-order motion correction, whether voxel-specific or volumetric models are used.

The parameters produced by our new SLOMOCO algorithm correlated with injected parameters (4836 timepoints) nearly as highly as the volumetric motion correlated with the volume-averaged injected motion (156 timepoints); however, considering that SLOMOCO produces the full timeseries of all slices and volumes, the correlation coefficient has a much higher significance. When including live subjects, the correlation and NMSE with the truth vectors is expected to diverge, as there is real motion in addition to the injected motion, and this is indeed what was observed (Table 4). The lowest mean tSTD was seen with the new slicewise model and either the TRU motion timeseries or the SLOMOCO timeseries.

In addition to our new slice motion model, we compared the Friston volumetric 12DOF model (S^{VOL}) and the Bullmore voxel-specific 12DOF model (S^{VOX}). Tellingly, the reduction in mean image tSTD in both cadavers and live subjects was about half as effective with the volumetric model as with the voxel-specific model (Tables 5 & 6, cadavers only column). With TRU regression or SLOMOCO with the new slice model, there was a reduction of 56%. These are substantial potential increases in detectability, if they translate directly to reduced noise level alone. For a simplistic illustration, if mean EPI signal level is 1000 and the noise level is 20, then a BOLD signal change of 1% is swamped by a noise level double its size. For an acquisition such as the one used here in a 4.5-cycle block paradigm experiment with 156 volumes, simulation shows that the linear correlation between the reference and a BOLD timecourse increases from 0.218 ($p=0.006$) at tSTD=20 to 0.261 ($p=0.00095$) at tSTD=15 and to 0.2912 ($p=0.00021$) at tSTD=12, corresponding to uncorrected, volumetric and voxel-specific regression respectively. In simple tests, this translates to the difference between surviving a search penalty of 160, 1000, and 5000, respectively. Real data and tests are not so simple, and data are typically smoothed for a variety of reasons. Nevertheless, the use of volumetric motion model comes with a significant cost to the correction efficiency and it should be avoided in favor of the more appropriate voxel-specific model in every case, as there is no cost to the user beyond additional care in setting up corrections.

In a similar vein, we showed that the use of a simplistic volumetric translations-only (VTD) motion metric(Van Dijk et al., 2012) is unsuitable for modeling the level of motion corruption in a dataset. Any motion analysis using translations alone to generate the motion metrics is likely to produce poor results. It may be expected that, because the correlations between translations and rotations is high, translations alone are sufficient for a metric of total displacement. Indeed, when using such metrics, where a single Euler angle and a single total translation are calculated from the 3 rotation and 3 translation parameters respectively(Van Dijk et al., 2012), the correlation between angle and translation is extremely high for FSL. This is partly because the conversion to rotations about the image corner results in a large portion of rotational motion appearing in the translation parameters. However, this does not mean that rotations and translations are thus equivalent, and our results show that this is not the case. The rotations are weighted arbitrarily by the distance from image center to the image corner and may be over-weighting rotations for most fields of view. Regardless, most in the field are unaware this is specific to one software tool, and using this same metric with center-based motion parameters will be more inappropriate because it will ignore rotations completely. We feel we must point out that using translations alone should be expected to result in lower sensitivity than using metrics based on the full 6 DOF and thus we strongly recommend against this.

Because of the limited sensitivity of volumetric metrics to intra-volume motion (see Fig 3), censoring using volumetric metrics cannot be expected to work reliably. It is possible previous studies reporting efficacious results after using censoring are reflective of reduced sensitivity, rather than effectiveness. It is difficult to draw conclusions from the use of censoring in real data due to the metrics that were used to identify motion corrupted volumes. It may be possible to use the SLOMOCO results to identify corrupted volumes, but this must be determined using a larger set of data with more variety in the injected motion. We point out that a justification often given for regression of global signal (or white matter or CSF signal) is the assumption that some or much of the motion artifact can be modeled in this way(Power et al.). This is not substantiated; as we demonstrate that the global signal has little to do with the motion-related signal changes at each voxel (Figs. 3 and 4) and therefore regressing global signal is not justified as a motion correction.

We did not assess a wider set of motion characterization methods, as these depend on having a variety of different motion parameters to inject, which was considered outside the scope of this study. We further point out our evaluation is naturally limited by the variety of motion induced in our data. We are attempting to study the effect on bias and sensitivity. Ideally one would inject motion that corresponds to real human head motion during tasks and rest. One possibility would be to acquire motion data in a mock (i.e., no static field) scanner using a commercial non-MRI tracker while subjects undergo a range of block-paradigm fMRI, event-related fMRI and RS-fMRI scans, and then inject this motion into later RS-fMRI scans of the same subjects in a real MRI. fMRI bias due to motion would be assessed by treating the RS-fMRI data as fMRI data and analyzing these data as if the subjects were performing the task. This data would also present a more thorough test of these motion correction methods as pertains to fMRI or RS-fMRI bias and sensitivity. This effort is outside the scope of this study, but we intend to follow up with such a study in the future. Motion-injection data acquired in live subjects will also contain unavoidable real, non-

injected head motion which will result in divergence from the ground truth. For this reason, data was only acquired in a few highly experienced subjects with known low motion performance. Live subject data were acquired to demonstrate comparability and as proof of principle for the type of study that would be needed to more fully assess BOLD sensitivity. For this study, we did not compare any sequence protocol parameters for motion artifact sensitivity, such as slice acquisition order, TR, flip angle and other parameters. It would be advantageous to use protocols that minimize motion artifacts, and we intend to follow this study with a protocol-optimization study using SimPACE.

Our evaluation of BOLD contamination was based solely on simulation, and this simulation showed that there was very small contamination from the BOLD activation in the motion metrics. The BOLD contamination in live subjects, whether from task or endogenous fluctuations, could be much higher as the simulations are likely somewhat inaccurately reflecting reality. BOLD contamination is a well-studied problem(Freire and Mangin, 2001; Freire et al., 2002) and solutions exist for some fMRI experiments, but when the paradigm is complex or unknown, as in the case of RS-fMRI, no solution exists. It may be possible to use ICA to denoise the data, considering BOLD fluctuations as the noise, and effectively de-BOLD the data, before estimation of the motion parameters. Subsequently, the de-BOLD estimated motion could be applied to the original data with less motion contamination. However, the full exploration and validation of such a method, is outside the scope of the present study.

In live subject data, the use of image tSTD as a metric for the comparison of methods is complicated by the existence of neuronal-related signal changes with a non-white temporal noise spectrum that we do not wish to reduce, and some neuronal signals will be correlated with motion as neuronal processes ultimately underlie head motion. The main problem with using tSTD as a metric is that any regression noise removal will also remove variance, regardless of the correctness of the model(Beall, 2010). If one were to compare a regression-based noise correction to no correction, one has to somehow account for the intrinsic reduction in variance through the reduction in degrees of freedom. However, by keeping the number of regressors the same across compared methods, this problem is largely avoided (but not completely, as the reduction in DOF is also dependent on the level of overlap, or non-orthogonality, between regressors; motion regressors typically overlap). One can also perform a Monte Carlo simulation of the effect of a given regression on a dataset’s variance using regression of random, arbitrary vectors as in (Beall and Lowe, 2010), but this was not necessary for our purposes as all comparisons were made across data with equal numbers of regressions performed.

SimPACE does not obtain signal changes due to receive-field contrast and changes in static-field homogeneity due to head position. However, in most of the brain these changes are typically smaller than partial volume and spin history motion effects, and for a relatively homogeneous coil both are likely to be smaller than the effect of motion on the phase-encode warping, which SimPACE does produce accurately. Furthermore, these can be accounted for or simulated retrospectively (Hartwig et al., 2011; Ooi et al., 2013; Xu et al., 2007), although this is outside the scope of the present study. Additionally, SimPACE does not produce within-slice acquisition motion or motion between excitation and completion of

EPI readout and thus is limited to between-slice motion. However, it is possible to induce or retrospectively simulate readout acquisition motion effects by adding spatially-varying phase to the raw k-space data(Bydder et al., 2002). It is unknown what the relative contribution of readout motion is with respect to all other sources of motion artifact. This could be studied with head motion tracking in a mock scanner setup.

There is considerable room for improvement to the SLOMOCO method. In particular, the outermost slices of the acquired volume are detected poorly by SLOMOCO. This is not surprising considering that the correction method relies on creating a template where the surrounding slices are motion-free. This can easily be dealt with, as long as one knows when setting up a protocol that the outermost slices will be at risk for motion. It may be possible to use adjacent slice information to improve or otherwise clean up the detected motion parameters for a given slice. Most head motion is slow enough that motion for a given slice should be reflected in the slices acquired before and after it. Then these two slices could be used to improve the motion estimation. In particular, the problem that SLOMOCO has with the outermost slices might be addressed in this manner. To fully understand the robustness of this method and the amount of head motion it is sensitive to, a study assessing a large sample of head tracker data and alreadyacquired MRI data is needed. In Figure 2, the injected and detected parameters are shown, and tellingly, there is some similarity over time in the smaller deviations from truth for some DOF in some slices. However, the per-slice accuracy correlations and MSE shown in Figure 6 shed more light on this situation. Figure 6a) shows that the spatially outermost slices have poor estimates with this method, and Figure 6b) shows that there is a nearly geometric relationship between accuracy and location within the volume. Figure 6c) breaks these data out by parameter and illustrates there is indeed a relative scaling factor variability across slices, that is probably reducing the effectiveness of the method. Given how the addition of an incorrect scaling parameter to any one DOF degrades the regression substantially, this may provide an effective avenue for improving the accuracy of motion estimates for each slice. At present time however, the use of SLOMOCO requires the discarding of the outermost slices. This can be accounted for in many cases when setting up a given acquisition protocol.

Head tracker systems for MRI may be useful for obtaining these motion parameters independently and would be invaluable for further validation and development of this method. However, given the accuracy with which SLOMOCO parameters represented the true motion vectors, and the difficulty experienced in translating early results into accurate head tracking, it is unclear whether head tracker data will be as accurate in obtaining parameters as accurate for regression as SLOMOCO. Adding 100-micron resolution noise to our injection timeseries resulted in a decrease in correlation between injection and injection +noise to 0.876 over 4836 timepoints (drop from a correlation of 1.0 when noise=0). This is comparable to the accuracy of the SLOMOCO z-translation parameters in Table 2 and suggests that SLOMOCO is accurate to approximately 100 microns or better.

It is important to point out that linear models of motion artifact are not entirely realistic. Spin history, warping and other effects are not linear, and are only approximately modeled by linear fitting. This is a major limitation of these regression methods, and will result in residual motion-related signal variance after correction.

Even with perfect modeling and removal of motion, there is typically still an effect on the resulting analysis(Bullmore et al., 1999). In task fMRI paradigms, any motion correlated with the stimulus will reduce the power of the experiment and effectively reduce the BOLD contrast-to-noise ratio (CNR). In RS-fMRI experiments, some low frequency BOLD fluctuations correlate with head motion because the head motion is ultimately neuronally derived. The characteristics of head motion will correlate with some of the resting state signal and thus, CNR of the connectivity measurement may also be reduced. This is a fundamental limitation of regression methods, that they cannot separate two covarying signals “correctly”. At best, they should assign equal variance to each covarying signal but this does not give the true proportion of variance due to each. Different experimental designs incorporating known signal perturbations or contrasts during acquisition, such as mixing paradigms or double-echo EPI, may be able to improve this situation. To produce analyses that are completely free of motion artifact, one should model the effective CNR due to the presence of motion on a subject-by-subject basis, in order to combine data with variability in BOLD detectability, as has been shown previously(Bullmore et al., 1999). Finally, even when using the injected motion vectors in the improved regression model, some motion artifact remains, at what appears to be an equivalent level in cadaver and live subject data. The regression model is still somewhat simplistic with respect to applicability to the T1 saturation effect and may therefore benefit from further modification.

Conclusions

The development and evaluation of motion correction methods for BOLD MRI have been hampered by the lack of realistic data accompanied by truth motion timeseries. SimPACE is an important step towards such gold-standard data. Insights obtained from these data led to the development of a new slice-wise motion detection and correction tool. SLOMOCO, a completely retrospective solution for head motion correction in BOLD-weighted MRI data, is a substantial new advance. We also demonstrate that motion metrics based on commonly used volumetric motion correction are not robust estimators of motion present in BOLD data.

Supplementary Material

Refer to Web version on PubMed Central for supplementary material.

Acknowledgments

The authors would like to gratefully acknowledge support from NIH grant 5P50NS038667-14 for the MRI acquisition of cadaver tissue, the assistance of Megan Griffiths in manuscript preparation and the staff of the Mellen Center for acquiring the cadaver data, including John Cowan, Tami Gaebelein, Sarah Gallucci and Derrek Tew. The authors would also like to gratefully acknowledge the contribution of the anonymous reviewers of this manuscript.

Abbreviations

0D	no derivative, absolute motion
1D	first derivative, relative motion

BOLD	blood oxygenation level-dependent
DOF	degrees of freedom
EPI	echoplanar imaging
FD	frame-wise displacement
fMRI	functional magnetic resonance imaging
GS	global signal
NMSE	normalized mean square error
PACE	Prospective Acquisition CorrEction
PGS	percent global signal
PV	partial volume
RF	radiofrequency
RMS	root mean square
ROI	region of interest
RS-fMRI	resting state fMRI
SLOMOCO	SLice-Oriented MOtion COrrection
SNR	signal-to-noise ratio
TD	total displacement
TR	repetition time
tSTD	temporal standard deviation
VTD	volumetric translations only.

Appendix

SimPACE

Modern MRI scanners include a method for semi-prospective head motion correction for EPI. Briefly, after each complete EPI volume is collected, a volumetric coregistration between the current volume and the first acquired volume is performed. The detected rigid-body motion parameters are then applied to transform the current acquisition coordinate system, which imparts an equivalent rigid-body translation and rotation of the tissue excited and read out by the sequence of gradient pulses in the pulse sequence. This allows the acquisition grid to follow the head motion at each volume and thereby remove accumulated motion, although instantaneous motion is still present. This was first described and implemented as Prospective Acquisition CorrEction (PACE)(Thesen et al., 2000). The SimPACE acquisition consists of two simple modifications. First, instead of motion being detected from the data, the motion parameters are read from a text file. Second, the gradient coordinate system is updated for every slice, rather than only at volume boundaries. In this way, instead of prospectively correcting for head motion, we can prospectively induce

arbitrary and highly accurate head motion independently for every slice and effectively simulate head motion effects (Fig 1). For discussion purposes, we follow the coordinate convention described in Figure 1 and use axial slices, such that×and y are in the plane of the acquisition, representing in-plane parameters, while z is the out-of-plane parameter. For the present study, the goal is to obtain motion-corruption with a portion relevant for unrealistic inter-volume motion (Fig 1a, lower left, and Fig 4) and a portion relevant for the more realistic scenario of intra-volume motion(Fig 1a, lower middle and right, and Fig 3), using the updating of gradients for each slice excitation and acquisition time.

Slice-accurate second-order motion model

There are several second-order motion regression models in use today that use volumetric motion parameters. The most commonly used model (Eqn 2 for $\mathbf{S^{VOL}}$) includes the 6 volumetric motion parameters and their squares. Some implementations include one-volume-delayed or first derivative of the parameters, to account for the spin history effect of an out-of-plane motion on the subsequent volume, but at the cost of more regressors (Friston et al., 1996). Note that ***x*** and ***xr*** represent translation along and rotation about the x-axis, respectively, of the entire volume. We refer to this model as the volumetric model of motion, because it does not model motion at each voxel independently but assumes that the volumetric motion represents voxel motion. Because of the variable location of each voxel with respect to the origin of rotation, this approximation will fail to model some of the motion-related signal. For example, a rotation of the axial slice about the axis perpendicular to it will result in opposite polarity displacements for voxels anterior and posterior to the center of rotation. If this is combined into a timeseries with many other arbitrary head motions, the resulting model will poorly fit signal changes due to motion. This model would be improved by conversion of the volumetric motion into voxel-specific translations, independently for each voxel. The voxel-specific model of $\mathbf{S^{VOX}}$ described in(Bullmore et al., 1999) and Eqn 3 converts the volumetric rotation and translation into individual voxel translation. The model as described includes the voxel translations, translations squared and copies of these vectors delayed by one volume to model spin history effect on the subsequent volume.

$$S_t^{VOL}=b_1\delta x_t+b_2(\delta x_t)^2+b_3\delta y_t+b_4(\delta y_t)^2+b_5\delta z_t+b_6(\delta z_t)^2+b_7\delta xr_t+b_8(\delta xr_t)^2+b_9\delta yr_t+b_{10}(\delta yr_t)^2 b_{11}\delta zr_t+b_{12}(\delta zr_t)^2 \quad \text{Eqn2}$$

The $\mathbf{S^{VOX}}$ model is sufficient for modeling motion known at the volumetric time resolution. However, to model motion known at the slice time resolution, this model must be modified to account for the motion of adjacent slices. Eqn 4 shows the slice-specific model of $\mathbf{S^{VOX\text{-}SLC}}$, incorporating ***zi*** and ***zs*** for the motion into this voxel of the adjacent inferior slice's voxel and the adjacent superior slice's voxel, respectively. Note that the delayed in-plane parameters (e.g., $\boldsymbol{dx_{t-1}}$, $\boldsymbol{dy_{t-1}}$, and their squares) have been removed, as we found that these parameters did not explain any additional variance over randomly generated regressors. Also note that parameters 7–10 in Eqn 4 are equivalent to (and identical to) parameters 11 & 12 in Eqn 3 when using volumetric parameters instead of slicewise parameters. Thus, with these adjustments, $\mathbf{S^{VOX\text{-}SLC}}$ can describe slicewise motion artifact signal in addition to artifact described by $\mathbf{S^{VOX}}$ while retaining the same total number of

regressors as the $\mathbf{S^{VOL}}$ and $\mathbf{S^{VOX}}$ models. A smaller number of regressors is useful because increased regressors reduce sensitivity(Beall, 2010). More details on slice acquisition order are provided in the supplementary material.

$$\begin{aligned} S_t^{VOX} = & b_1\delta x_t \\ & + b_2(\delta x_t)^2 + b_3\delta y_t \\ & + b_4(\delta y_t)^2 + b_5\delta z_t \\ & + b_6(\delta z_t)^2 + b_7\delta x_{t-1} \\ & + b_8(\delta x_{t-1})^2 + b_9\delta y_{t-1} \\ & + b_{10}(\delta y_{t-1})^2 + b_{11}\delta z_{t-1} \\ & + b_{12}(\delta z_{t-1})^2 \end{aligned} \qquad \text{Eqn3}$$

$$\begin{aligned} S_t^{VOX-SLC} = & b_1\delta x_t \\ & + b_2(\delta x_t)^2 + b_3\delta y_t \\ & + b_4(\delta y_t)^2 + b_5\delta z_t \\ & + b_6(\delta z_t)^2 + b_7\delta zi_{t-1} \\ & + b_8(\delta zi_{t-1})^2 \\ & + b_9\delta zs_{t-1} \\ & + b_{10}(\delta zs_{t-1})^2 \\ & + b_{11}\delta z_{t-1} \\ & + b_{12}(\delta z_{t-1})^2 \end{aligned} \qquad \text{Eqn4}$$

Slice-accurate motion parameters

As discussed in the introduction, we are unaware of a slice-to-volume coregistration method for BOLD EPI that removes the timeseries motion artifact due to slicewise motion. Our method, SLice-Oriented MOtion COrrection (SLOMOCO), is not a coregistration technique, but a motion estimation and subsequent correction through regression. We will show that, with our implementation, we observe motion estimates that correlate very strongly to the true motion over an EPI dataset. The estimator amplitudes we observe are incorrect, which precludes its use for slice-to-volume regridding, but because linear regression is insensitive to amplitude, this drawback does not preclude a highly effective regression-based correction. Thus, these motion estimates can be used as regressors in a slice-accurate motion model as described above. Here we describe our algorithm:

1. The data are first corrected for in-plane motion by independently coregistering each slice to the mean over time, while keeping the 3 out-of-plane DOF fixed to zero. This step is not novel and implementations exist. This is hereafter referred to as slicewise in-plane motion correction.
2. For each in-plane-corrected slice, a 3D+time dataset is constructed around this slice of interest by freezing the motion on all other slices. All other slice data is replaced with the mean image, replicated for each volume, except for the slice of interest,

which is unchanged. These 3D+time datasets (one per slice) is then blurred with a 3mm full-width-half-maximum 3D Gaussian spatial filter. In each resulting slice dataset, there is no temporal variance except on the slice that is not frozen.

3. For each slice dataset, a volumetric coregistration is performed over time using the mean 3D image as the registration target (the mean image is not blurred), resulting in a timeseries of independent motion parameters for each slice dataset. The set of slice motion parameters obtained are then used without any further processing as the estimators of the slicewise motion.

Note that this algorithm treats in-plane and out-of-plane motion differently. Because of the 2D acquisition, in-plane and out-of-plane motion produce different signal artifacts. In-plane motion primarily induces partial volume effects and in some regions B0 and B1 effects, whereas out-of-plane motion is primarily a combination of spin history and partial volume effects. The SLOMOCO method assumes that there is no cumulative motion, thus either the data must be acquired using a prospective motion acquisition strategy or a retrospective volumetric correction must be performed prior to this algorithm. This is important because otherwise any residual partial volume effects on real BOLD signal changes will affect fMRI and connectivity analyses. Because it is not possible to cleanly separate signal changes due to neuronal changes, partial volume and spin history effects, a *partial volume correction for out-of-plane motion would introduce as much or more signal artifact than would be seen without out-of-plane partial volume correction*. Our data show that the regression model is the most effective way, of those considered, to remove artifact due to out-of-plane motion.

Second-order model and slice acquisition order

To model effects of spin history from voxels in adjacent slices on the present voxel, it is necessary to include motion of those voxels into the present voxel. For interleaved acquisitions, the temporal index of the adjacent slice motion is different for slices acquired in the first temporal half (TR/2) or second half of the interleaved volume. Eqn 4 used previous temporal indices (t-1) for adjacent slice effects. This is only true for slices acquired in the first half of the acquisition, because these are affected by motion of adjacent slices that occurred during the previous volume. Thus, one should use Eqn 4 for the first half slices acquired in an interleaved acquisition, this is repeated here as Eqn 5: $\mathbf{S(1^{st}\text{-}half)^{VOX\text{-}SLC}}$. To model these effects for slices acquired in the second half of the volume, it is necessary to include current temporal indices (t) for adjacent slice effects. This is shown in Eqn 6 for $\mathbf{S(2^{nd}\text{-}half)^{VOX\text{-}SLC}}$. The use of both Eqn 5 and 6 depending on which slice we are modeling, will correctly account for whether the present slice timepoint occurs before or after the acquisition of the 2 adjacent slices. Our algorithm appropriately alternates between these two depending on the number of slices and the current slice number within the volume (on Siemens EPI sequences, an even number of slices is acquired starting with the first even slice, or slice number 2, while for an odd number of slices, the first acquired slice is the first, most inferior slice).

$$\begin{aligned} S(1st-half)_t^{VOX-SLC} \\ =&b_1\delta x_t \\ &+b_2(\delta x_t)^2+b_3\delta y_t \\ &+b_4(\delta y_t)^2+b_5\delta z_t \\ &+b_6(\delta z_t)^2+b_7\delta zi_{t-1} \\ &+b_8(\delta zi_{t-1})^2 \\ &+b_9\delta zs_{t-1} \\ &+b_{10}(\delta zs_{t-1})^2 \\ &+b_{11}\delta z_{t-1} \\ &+b_{12}(\delta z_{t-1})^2 \end{aligned} \quad \text{Eqn5}$$

$$\begin{aligned} S(2nd-half)_t^{VOX-SLC} \\ =&b_1\delta x_t \\ &+b_2(\delta x_t)^2+b_3\delta y_t \\ &+b_4(\delta y_t)^2+b_5\delta z_t \\ &+b_6(\delta z_t)^2+b_7\delta zi_t \\ &+b_8(\delta zi_t)^2+b_9\delta zs_t \\ &+b_{10}(\delta zs_t)^2+b_{11}\delta z_{t-1} \\ &+b_{12}(\delta z_{t-1})^2 \end{aligned} \quad \text{Eqn6}$$

For sequential ascending acquisition of axial slices, it is necessary to include motion in the superior direction of the inferior slice's voxel that lies immediately beneath the present voxel for which we are modeling motion (δzi_t), as that motion will steal signal from the subsequent acquisition of the present slice's voxel. It is also important to include any motion in the inferior direction of the superior slice's voxel immediately adjacent and above the present voxel under analysis, occurring during the previous volume (δzs_{t-1}) as shown in Eqn 7. This relates to signal stealing from the previous volume when the superior slice was being acquired. For ascending sequential acquisition, the effect of the inferior adjacent slice is much greater than the effect of the superior adjacent slice and somewhat greater than the present slice's out-of-plane motion, because the temporal disturbance of the sampling grid is so much greater. Any inferior slice motion into the present voxel disrupts the sampling from TR-to-TR into TR-to-TR/zdim and then potentially back to TR. Meanwhile, any superior slice motion produces a much smaller temporal disruption from TR-to-TR into TR-to- (TR-TR/zdim). This model must be modified further for arbitrary slice timing, which we do not cover here. We only point out that the relative importance of an adjacent voxel's motion into the present voxel is dependent on the timing relative to the present voxel and how this motion would disrupt the acquisition timing.

$$
\begin{aligned}
S(seq)_t^{VOX-SLC} \\
&= b_1\delta x_t \\
&+ b_2(\delta x_t)^2 + b_3\delta y_t \\
&+ b_4(\delta y_t)^2 + b_5\delta z_t \\
&+ b_6(\delta z_t)^2 + b_7\delta zi_t \\
&+ b_8(\delta zi_t)^2 + b_9\delta zs_{t-1} \\
&+ b_{10}(\delta zs_{t-1})^2 \\
&+ b_{11}\delta z_{t-1} \\
&+ b_{12}(\delta z_{t-1})^2
\end{aligned}
\qquad \text{Eqn7}
$$

Bibliography

Aksoy M, Forman C, Straka M, Cukur T, Hornegger J, Bammer R. Hybrid prospective and retrospective head motion correction to mitigate cross-calibration errors. Magn Reson Med. 2012; 67:1237–1251. [PubMed: 21826729]

Andersson JL, Hutton C, Ashburner J, Turner R, Friston K. Modeling geometric deformations in EPI time series. Neuroimage. 2001; 13:903–919. [PubMed: 11304086]

Ardekani BA, Bachman AH, Helpern JA. A quantitative comparison of motion detection algorithms in fMRI. Magn Reson Imaging. 2001; 19:959–963. [PubMed: 11595367]

Beall E, Lowe M, Alberts JL, Frankemolle AM, Thota AK, Shah C, Phillips MD. The Effect of Forced-Exercise Therapy for Parkinson's Disease on Motor Cortex Functional Connectivity. Brain Connect. 2013

Beall EB. Adaptive cyclic physiologic noise modeling and correction in functional MRI. J Neurosci Methods. 2010; 187:216–228. [PubMed: 20096307]

Beall EB, Lowe MJ. Isolating physiologic noise sources with independently determined spatial measures. Neuroimage. 2007; 37:1286–1300. [PubMed: 17689982]

Beall EB, Lowe MJ. The non-separability of physiologic noise in functional connectivity MRI with spatial ICA at 3T. J Neurosci Methods. 2010; 191:263–276. [PubMed: 20600313]

Bullmore ET, Brammer MJ, Rabe-Hesketh S, Curtis VA, Morris RG, Williams SC, Sharma T, McGuire PK. Methods for diagnosis and treatment of stimulus-correlated motion in generic brain activation studies using fMRI. Hum Brain Mapp. 1999; 7:38–48. [PubMed: 9882089]

Bydder M, Larkman DJ, Hajnal JV. Detection and elimination of motion artifacts by regeneration of k-space. Magn Reson Med. 2002; 47:677–686. [PubMed: 11948728]

Cox RW. AFNI: software for analysis and visualization of functional magnetic resonance neuroimages. Comput Biomed Res. 1996; 29:162–173. [PubMed: 8812068]

Cox RW, Jesmanowicz A. Real-time 3D image registration for functional MRI. Magn Reson Med. 1999; 42:1014–1018. [PubMed: 10571921]

Derbyshire JA, Wright GA, Henkelman RM, Hinks RS. Dynamic scan-plane tracking using MR position monitoring. J Magn Reson Imaging. 1998; 8:924–932. [PubMed: 9702895]

Dold C, Zaitsev M, Speck O, Firle EA, Hennig J, Sakas G. Prospective head motion compensation for MRI by updating the gradients and radio frequency during data acquisition. Med Image Comput Comput Assist Interv. 2005; 8:482–489. [PubMed: 16685881]

Dold C, Zaitsev M, Speck O, Firle EA, Hennig J, Sakas G. Advantages and limitations of prospective head motion compensation for MRI using an optical motion tracking device. Acad Radiol. 2006; 13:1093–1103. [PubMed: 16935721]

Drangova M, Bowman B, Pelc N. Physiologic motion phantom for MRI applications. J Magn Reson Imaging. 1996; 6:513–518. [PubMed: 8724418]

Drobnjak I, Gavaghan D, Suli E, Pitt-Francis J, Jenkinson M. Development of a functional magnetic resonance imaging simulator for modeling realistic rigid-body motion artifacts. Magn Reson Med. 2006; 56:364–380. [PubMed: 16841304]

Field AS, Yen YF, Burdette JH, Elster AD. False cerebral activation on BOLD functional MR images: study of low-amplitude motion weakly correlated to stimulus. AJNR Am J Neuroradiol. 2000; 21:1388–1396. [PubMed: 11003269]

Fisher E, Chang A, Fox RJ, Tkach JA, Svarovsky T, Nakamura K, Rudick RA, Trapp BD. Imaging correlates of axonal swelling in chronic multiple sclerosis brains. Ann Neurol. 2007; 62:219–228. [PubMed: 17427920]

Foerster BU, Tomasi D, Caparelli EC. Magnetic field shift due to mechanical vibration in functional magnetic resonance imaging. Magn Reson Med. 2005; 54:1261–1267. [PubMed: 16215962]

Forman C, Aksoy M, Hornegger J, Bammer R. Self-encoded marker for optical prospective head motion correction in MRI. Med Image Comput Comput Assist Interv. 2010; 13:259–266. [PubMed: 20879239]

Fox MD, Zhang D, Snyder AZ, Raichle ME. The global signal and observed anticorrelated resting state brain networks. J Neurophysiol. 2009; 101:3270–3283. [PubMed: 19339462]

Freire L, Mangin JF. Motion correction algorithms may create spurious brain activations in the absence of subject motion. Neuroimage. 2001; 14:709–722. [PubMed: 11506543]

Freire L, Roche A, Mangin JF. What is the best similarity measure for motion correction in fMRI time series? IEEE Trans Med Imaging. 2002; 21:470–484. [PubMed: 12071618]

Friston KJ, Ashburner J, Frith CD, Poline JB, Heather JD, Frackowiak RS. Spatial Registration and Normalization of Images. Human Brain Mapping. 1995; 2:165–189.

Friston KJ, Williams S, Howard R, Frackowiak RS, Turner R. Movement-related effects in fMRI time-series. Magn Reson Med. 1996; 35:346–355. [PubMed: 8699946]

Gunther M, Feinberg DA. Ultrasound-guided MRI: preliminary results using a motion phantom. Magn Reson Med. 2004; 52:27–32. [PubMed: 15236363]

Hajnal JV, Myers R, Oatridge A, Schwieso JE, Young IR, Bydder GM. Artifacts due to stimulus correlated motion in functional imaging of the brain. Magn Reson Med. 1994; 31:283–291. [PubMed: 8057799]

Hajnal JV, Saeed N, Oatridge A, Williams EJ, Young IR, Bydder GM. Detection of subtle brain changes using subvoxel registration and subtraction of serial MR images. J Comput Assist Tomogr. 1995; 19:677–691. [PubMed: 7560311]

Hallquist MN, Hwang K, Luna B. The nuisance of nuisance regression: spectral misspecification in a common approach to resting-state fMRI preprocessing reintroduces noise and obscures functional connectivity. Neuroimage. 2013; 82:208–225. [PubMed: 23747457]

Hartwig A, Engstron M, Flodmark O, Invgar M, Skare S. A simple method to reduce signal fluctuations in fMRI caused by the interaction between motion and coil sensitivities. Proceedings of the International Society for Magnetic Resonance in Medicine, Montreal. 2011

He H, Liu TT. A geometric view of global signal confounds in resting-state functional MRI. Neuroimage. 59:2339–2348. [PubMed: 21982929]

Herbst M, Maclaren J, Lovell-Smith C, Sostheim R, Egger K, Harloff A, Korvink J, Hennig J, Zaitsev M. Reproduction of motion artifacts for performance analysis of prospective motion correction in MRI. Magn Reson Med. 71:182–190. http://www.fil.ion.ucl.ac.uk/spm, W.D.o.C.N., SPM99. [PubMed: 23440737]

Huber ME, Stuber M, Botnar RM, Boesiger P, Manning WJ. Low-cost MR-compatible moving heart phantom. J Cardiovasc Magn Reson. 2000; 2:181–187. [PubMed: 11545115]

Jenkinson M, Bannister P, Brady M, Smith S. Improved optimization for the robust and accurate linear registration and motion correction of brain images. Neuroimage. 2002; 17:825–841. [PubMed: 12377157]

Jezzard P, Clare S. Sources of distortion in functional MRI data. Hum Brain Mapp. 1999; 8:80–85. [PubMed: 10524596]

Jiang A, Kennedy DN, Baker JR, Weisskoff RM, Tootell RBH, Woods RP, Benson RR, Kwong KK, Brady TJ, Rosen BR, Belliveau JW. Motion detection and correction in functional MR imaging. Human Brain Mapping. 1995; 3:224–235.

Jo HJ, Saad ZS, Simmons WK, Milbury LA, Cox RW. Mapping sources of correlation in resting state FMRI, with artifact detection and removal. Neuroimage. 52:571–582. [PubMed: 20420926]

Johnstone T, Ores Walsh KS, Greischar LL, Alexander AL, Fox AS, Davidson RJ, Oakes TR. Motion correction and the use of motion covariates in multiple-subject fMRI analysis. Hum Brain Mapp. 2006; 27:779–788. [PubMed: 16456818]

Kim B, Boes JL, Bland PH, Chenevert TL, Meyer CR. Motion correction in fMRI via registration of individual slices into an anatomical volume. Magn Reson Med. 1999; 41:964–972. [PubMed: 10332880]

Kober T, Gruetter R, Krueger G. Prospective and retrospective motion correction in diffusion magnetic resonance imaging of the human brain. Neuroimage. 2012; 59:389–398. [PubMed: 21763773]

Lee CC, Grimm RC, Manduca A, Felmlee JP, Ehman RL, Riederer SJ, Jack CR Jr. A prospective approach to correct for inter-image head rotation in fMRI. Magn Reson Med. 1998; 39:234–243. [PubMed: 9469706]

Leung G, Plewes DB. Retrospective motion compensation using variable-density spiral trajectories. J Magn Reson Imaging. 2005; 22:373–380. [PubMed: 16104023]

Lund TE, Norgaard MD, Rostrup E, Rowe JB, Paulson OB. Motion or activity: their role in intra- and inter-subject variation in fMRI. Neuroimage. 2005; 26:960–964. [PubMed: 15955506]

Maclaren J, Armstrong BS, Barrows RT, Danishad KA, Ernst T, Foster CL, Gumus K, Herbst M, Kadashevich IY, Kusik TP, Li Q, Lovell-Smith C, Prieto T, Schulze P, Speck O, Stucht D, Zaitsev M. Measurement and correction of microscopic head motion during magnetic resonance imaging of the brain. PLoS One. 2012; 7:e48088. [PubMed: 23144848]

Morgan VL, Dawant BM, Li Y, Pickens DR. Comparison of fMRI statistical software packages and strategies for analysis of images containing random and stimuluscorrelated motion. Comput Med Imaging Graph. 2007; 31:436–446. [PubMed: 17574816]

Morgan VL, Pickens DR, Hartmann SL, Price RR. Comparison of functional MRI image realignment tools using a computer-generated phantom. Magn Reson Med. 2001; 46:510–514. [PubMed: 11550243]

Muresan L, Renken R, Roerdink JB, Duifhuis H. Automated correction of spin-history related motion artefacts in fMRI: simulated and phantom data. IEEE Trans Biomed Eng. 2005; 52:1450–1460. [PubMed: 16119241]

Murphy K, Birn RM, Handwerker DA, Jones TB, Bandettini PA. The impact of global signal regression on resting state correlations: are anti-correlated networks introduced? Neuroimage. 2009; 44:893–905. [PubMed: 18976716]

Oakes TR, Johnstone T, Ores Walsh KS, Greischar LL, Alexander AL, Fox AS, Davidson RJ. Comparison of fMRI motion correction software tools. Neuroimage. 2005; 28:529–543. [PubMed: 16099178]

Ooi MB, Krueger S, Thomas WJ, Swaminathan SV, Brown TR. Prospective real-time correction for arbitrary head motion using active markers. Magn Reson Med. 2009; 62:943–954. [PubMed: 19488989]

Ooi MB, Muraskin J, Zou X, Thomas WJ, Krueger S, Aksoy M, Bammer R, Brown TR. Combined prospective and retrospective correction to reduce motion-induced image misalignment and geometric distortions in EPI. Magn Reson Med. 2013; 69:803–811. [PubMed: 22499027]

Pandey, KK. Biomedical Engineering. Ann Arbor: University of Michigan; 2009. Mitigation of Motion Artifacts in Functional MRI: A Combined Acquisition, Reconstruction and Post Processing Approach; p. 127

Pfeuffer J, Van de Moortele PF, Ugurbil K, Hu X, Glover GH. Correction of physiologically induced global off-resonance effects in dynamic echo-planar and spiral functional imaging. Magn Reson Med. 2002; 47:344–353. [PubMed: 11810679]

Power JD, Barnes KA, Snyder AZ, Schlaggar BL, Petersen SE. Spurious but systematic correlations in functional connectivity MRI networks arise from subject motion. Neuroimage. 2011; 59:2142–2154. [PubMed: 22019881]

Power JD, Mitra A, Laumann TO, Snyder AZ, Schlaggar BL, Petersen SE. Methods to detect, characterize, and remove motion artifact in resting state fMRI. Neuroimage. 84C:320–341.

Qin L, van Gelderen P, Derbyshire JA, Jin F, Lee J, de Zwart JA, Tao Y, Duyn JH. Prospective head-movement correction for high-resolution MRI using an in-bore optical tracking system. Magn Reson Med. 2009; 62:924–934. [PubMed: 19526503]

Raj D, Anderson AW, Gore JC. Respiratory effects in human functional magnetic resonance imaging due to bulk susceptibility changes. Phys Med Biol. 2001; 46:3331–3340. [PubMed: 11768509]

Raj D, Paley DP, Anderson AW, Kennan RP, Gore JC. A model for susceptibility artefacts from respiration in functional echo-planar magnetic resonance imaging. Phys Med Biol. 2000; 45:3809–3820. [PubMed: 11131201]

Roche A. A four-dimensional registration algorithm with application to joint correction of motion and slice timing in fMRI. IEEE Trans Med Imaging. 2011; 30:1546–1554. [PubMed: 21427017]

Saad ZS, Gotts SJ, Murphy K, Chen G, Jo HJ, Martin A, Cox RW. Trouble at rest: how correlation patterns and group differences become distorted after global signal regression. Brain Connect. 2:25–32. [PubMed: 22432927]

Satterthwaite TD, Wolf DH, Loughead J, Ruparel K, Elliott MA, Hakonarson H, Gur RC, Gur RE. Impact of in-scanner head motion on multiple measures of functional connectivity: relevance for studies of neurodevelopment in youth. Neuroimage. 60:623–632. [PubMed: 22233733]

Scholvinck ML, Maier A, Ye FQ, Duyn JH, Leopold DA. Neural basis of global resting-state fMRI activity. Proc Natl Acad Sci U S A. 2010; 107:10238–10243. [PubMed: 20439733]

Sheltraw D, Inglis B. A simulation of the effects of receive field contrast on motion-corrected EPI time series. 2012 Oct 12. arXiv:med-ph/1210.3633v1.

Smith SM, Jenkinson M, Woolrich MW, Beckmann CF, Behrens TE, Johansen-Berg H, Bannister PR, De Luca M, Drobnjak I, Flitney DE, Niazy RK, Saunders J, Vickers J, Zhang Y, De Stefano N, Brady JM, Matthews PM. Advances in functional and structural MR image analysis and implementation as FSL. Neuroimage. 2004; 23(Suppl 1):S208–S219. [PubMed: 15501092]

Thesen S, Heid O, Mueller E, Schad LR. Prospective acquisition correction for head motion with image-based tracking for real-time fMRI. Magn Reson Med. 2000; 44:457–465. [PubMed: 10975899]

Van de Moortele PF, Pfeuffer J, Glover GH, Ugurbil K, Hu X. Respiration-induced B0 fluctuations and their spatial distribution in the human brain at 7 Tesla. Magn Reson Med. 2002; 47:888–895. [PubMed: 11979567]

Van Dijk KR, Sabuncu MR, Buckner RL. The influence of head motion on intrinsic functional connectivity MRI. Neuroimage. 2012; 59:431–438. [PubMed: 21810475]

Woods RP, Cherry SR, Mazziotta JC. Rapid automated algorithm for aligning and reslicing PET images. J Comput Assist Tomogr. 1992; 16:620–633. [PubMed: 1629424]

Wu DH, Lewin JS, Duerk JL. Inadequacy of motion correction algorithms in functional MRI: role of susceptibility-induced artifacts. J Magn Reson Imaging. 1997; 7:365–370. [PubMed: 9090592]

Xu N, Fitzpatrick JM, Li Y, Dawant BM, Pickens DR, Morgan VL. Computer-generated fMRI phantoms with motion-distortion interaction. Magn Reson Imaging. 2007; 25:1376–1384. [PubMed: 17583462]

Yancey SE, Rotenberg DJ, Tam F, Chiew M, Ranieri S, Biswas L, Anderson KJ, Baker SN, Wright GA, Graham SJ. Spin-history artifact during functional MRI: potential for adaptive correction. Med Phys. 2011; 38:4634–4646. [PubMed: 21928636]

Zaitsev M, Dold C, Sakas G, Hennig J, Speck O. Magnetic resonance imaging of freely moving objects: prospective real-time motion correction using an external optical motion tracking system. Neuroimage. 2006; 31:1038–1050. [PubMed: 16600642]

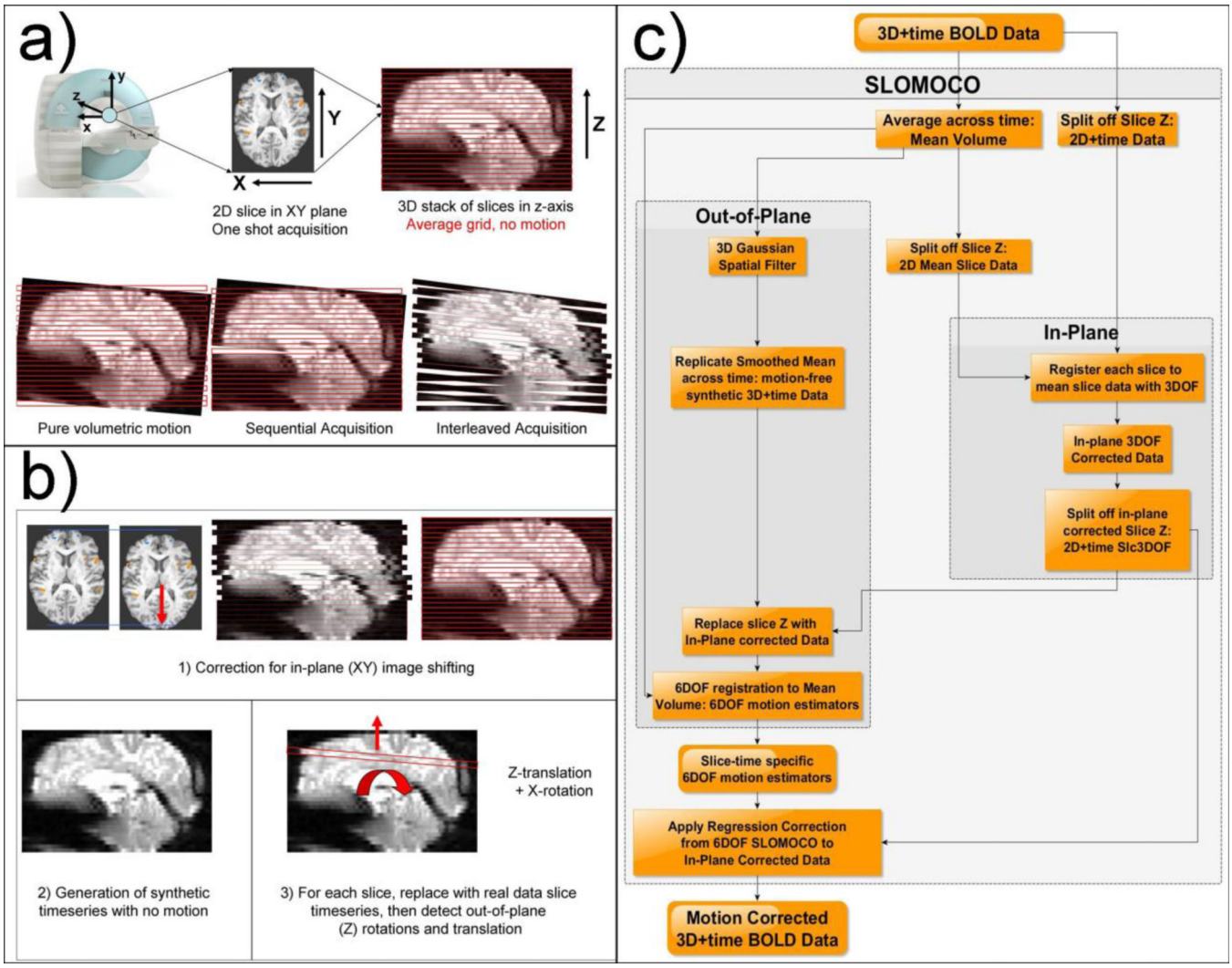

Fig. 1.

Schematic of slicewise motion detection algorithm, a) schematic of volumetric motion synchronized to the volume, motion part-way through volume acquisition in a sequential acquisition and motion during an interleaved acquisition, b) SLOMOCO algorithm graphic and c) SLOMOCO flowchart diagram.

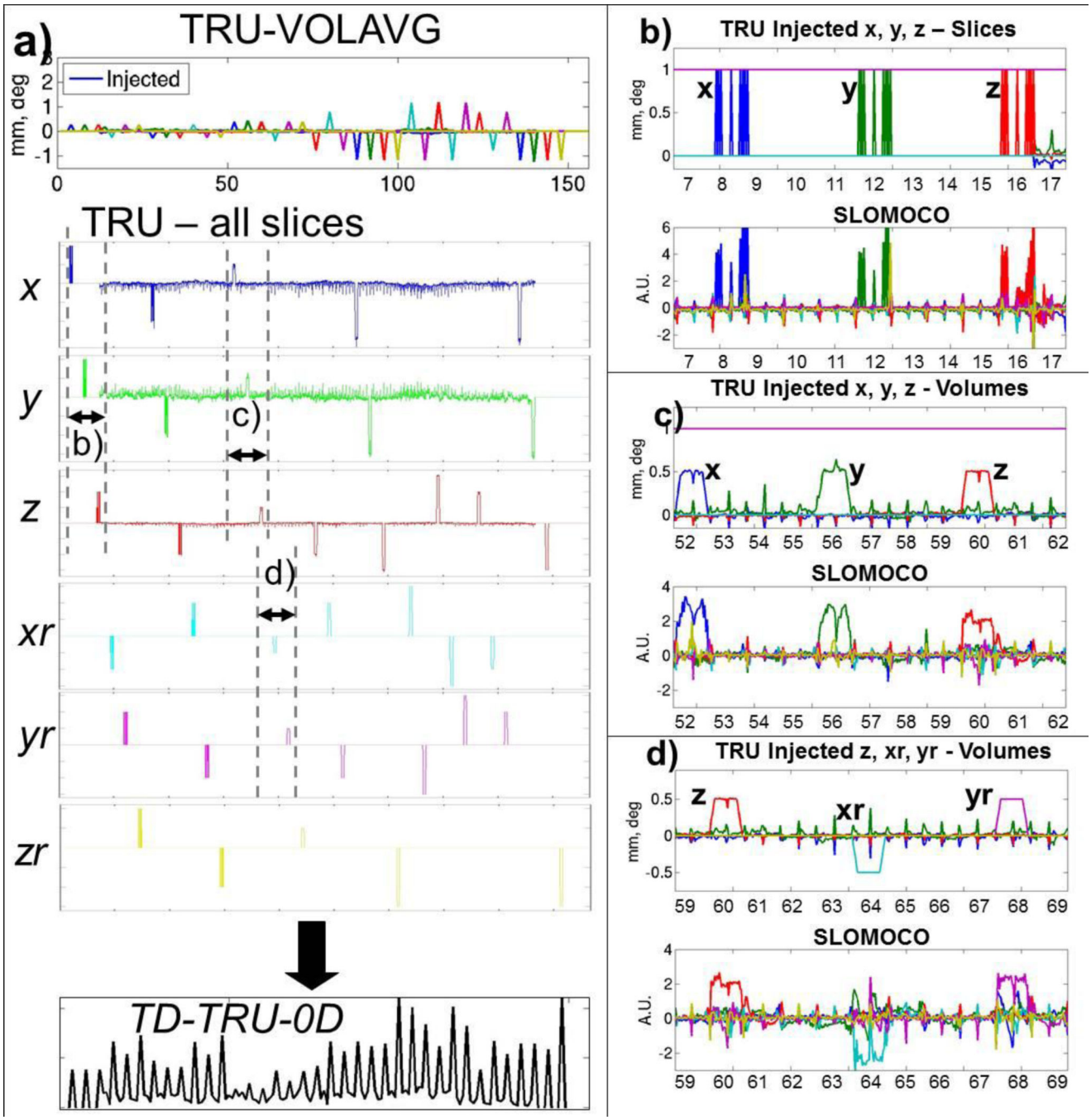

Fig. 2.

Injected motion timeseries, metric based on slicewise known motion, and selected portions showing performance of SLOMOCO at detecting slicewise motion. A) TRU-AVG, TRU (separated by DOF) and TD-TRU-0D. B) First selected time shows injection of x-, y-, and z-translation spikes of 1 mm on 10 independent, nonadjacent (temporal or spatial) slices. B) Second selected time shows x-, y-, and z-translation spikes on volumes. C) Injection including last z-translation and x- and y-rotations, representing all 3 critical out-of-plane DOF. Major deviation from injected motion exists almost exclusively on the 1 most inferior

and the 2 most superior slices. Colors: blue = x-translation, green = y-translation, red = z-translation, cyan = xrotation, purple = y-rotation.

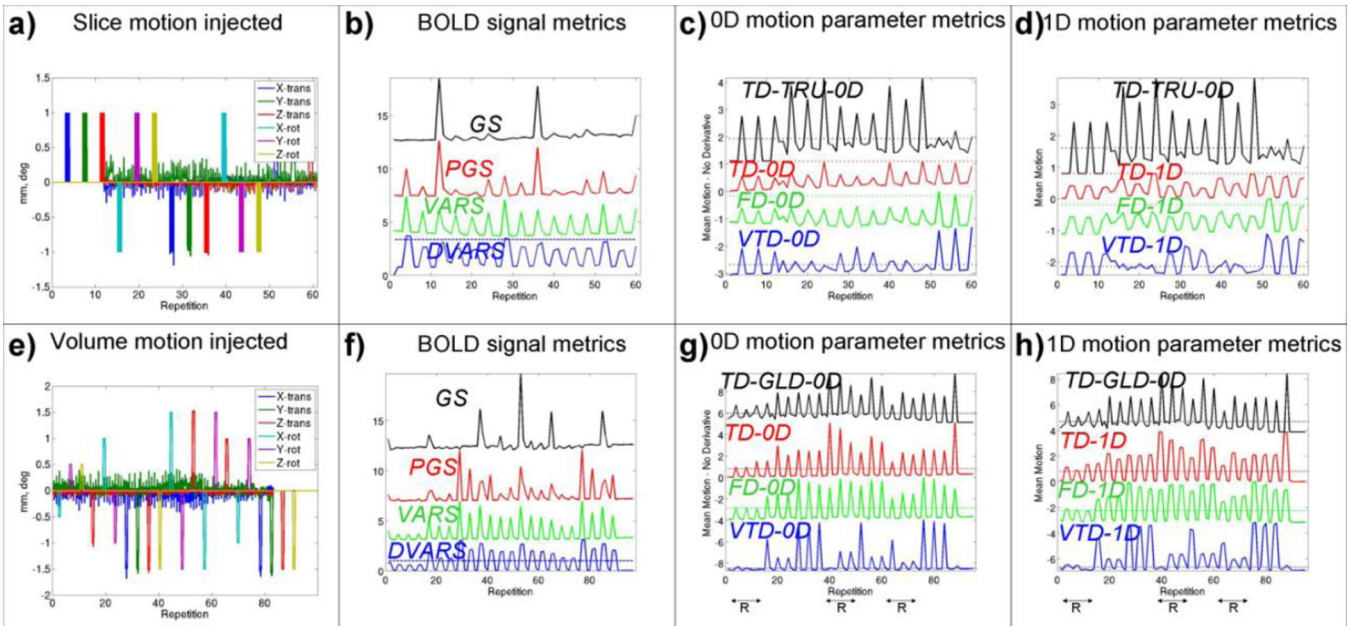

Fig. 3.

Motion metrics for realistic (top row, motion injected on 10 nonadjacent slices) slice-wise injected motion and unrealistic (bottom row, motion injected for all slices within a volume) volume injected motion. Far left (a,e) show injected motion parameters. Top row consists of first 50 volumes of SimPACE scan shown in Fig 2 left panel and bottom row consists of last 100 volumes of same scan. A) slicewise and E) volumetric injected motion, B,F) GS, PGS, VARS and DVARS BOLD signal-based metrics. C,G) No-derivative (TD-0D, FD-0D, VTD-0D) volumetric motion parameter based motion metrics and slicewise injected motion metric (TDTRU-0D). D,H) First-derivative (TD-1D, FD-1D, VTD-1D) motion metrics and slicewise motion (0^{th} derivative). Dotted and colored thresholds based on literature are also shown for each metric (0.5 for BOLD signal-based metrics, 0.5 for TD, FD and 0.1 for VTD), demonstrating the failure of volumetric motion parameter-based or BOLD signal-based motion detection methods to appropriately flag slice-wise motion. Segments of volumetric injection with rotational motion impulses injected are indicated with R at bottom of G) and H). Metrics are displayed separated by individual maxima and minima. For zoomed detail and overlay, see Fig 4. Vectors were normalized and plotted spaced for visualization only.

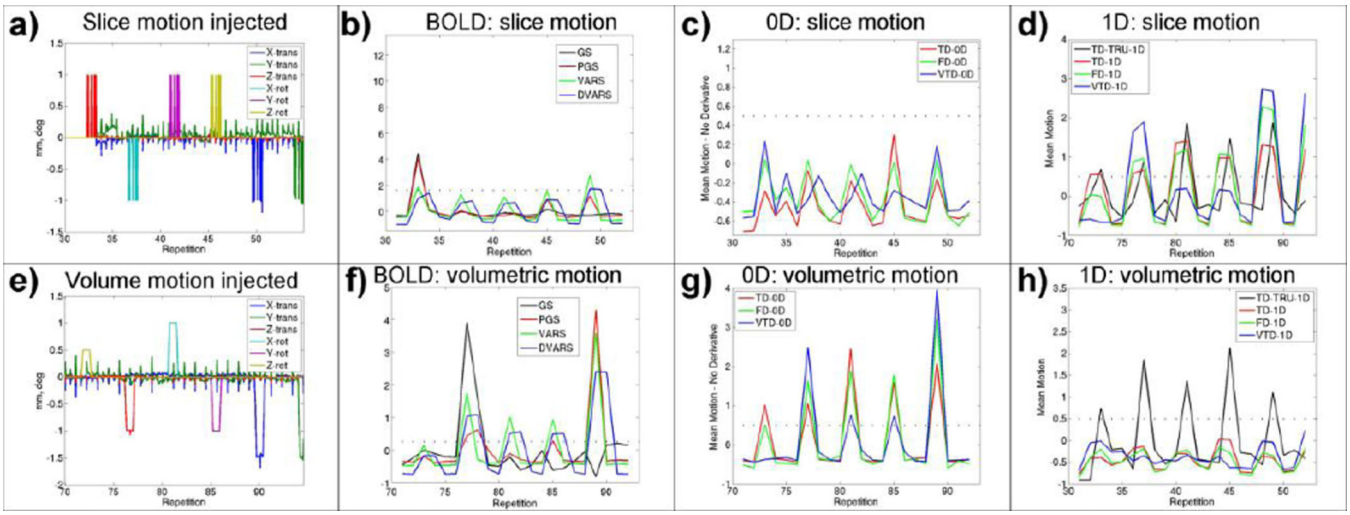

Fig. 4.

Selected segment of Fig 3, zoomed to show detail. Metrics are displayed overlain. Note in zoomed view of slicewise injection in A) individual slice timepoints can be observed, with 1mm z-translation injection occurring over 10 nonadjacent slices within volume 32, followed by xrotation injection on 10 slices in volume 36, and so on (every 4th volume). Similarly, the zoomed view of volumetric injection in E) shows injection of 0.5 degrees z-rotation motion on all slices of volume 72, followed by -1mm z-translation on all slices of volume 76, and so on. Vectors were normalized and plotted spaced for visualization only.

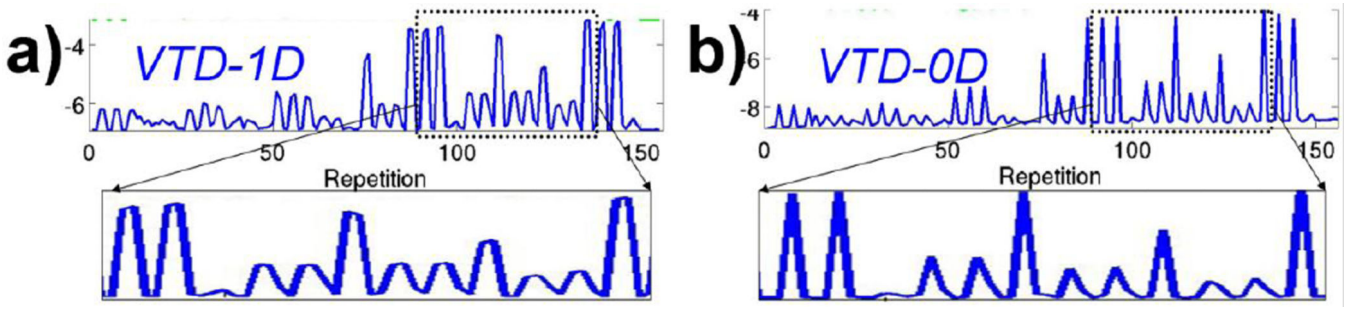

Fig. 5.

Detail of VTD-1D and VTD-0D, demonstrating the derivative-based metrics suffer from nearly equal levels of assigned motion on two adjacent volumes, despite the motion occurring only on one volume. Vectors were normalized and plotted spaced for visualization only.

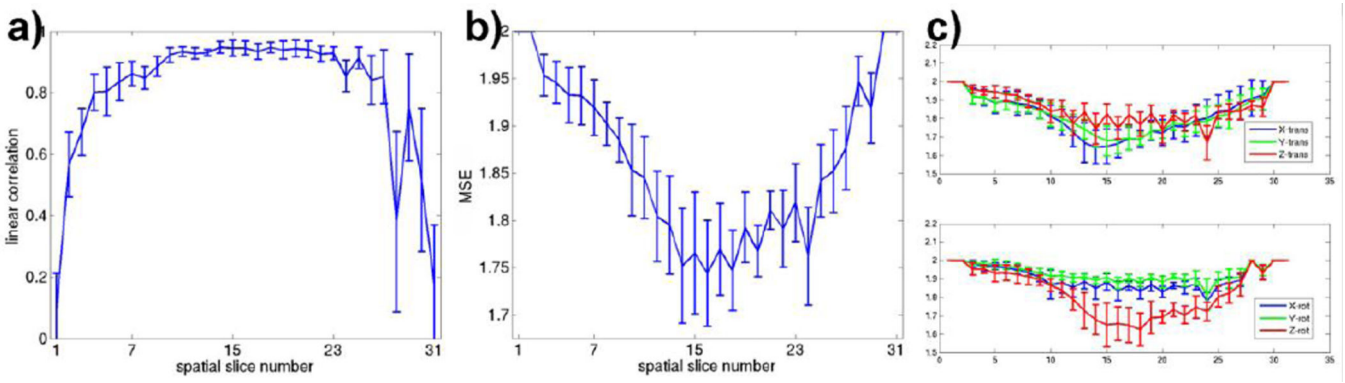

Fig. 6.

A) Pearson linear correlation versus temporal slice number (interleaved ascending acquisition: slicetime 1 = slice 1, slicetime 16 = slice 31, slicetime 31 = slice 30). B) MSE versus temporal slice number. C) Breakout of (B) by each DOF, with translations on top and rotations on bottom. The most inferior slice and the 2 most superior slices exhibit poor correlation in the presence of very strong correlation for all other slices.

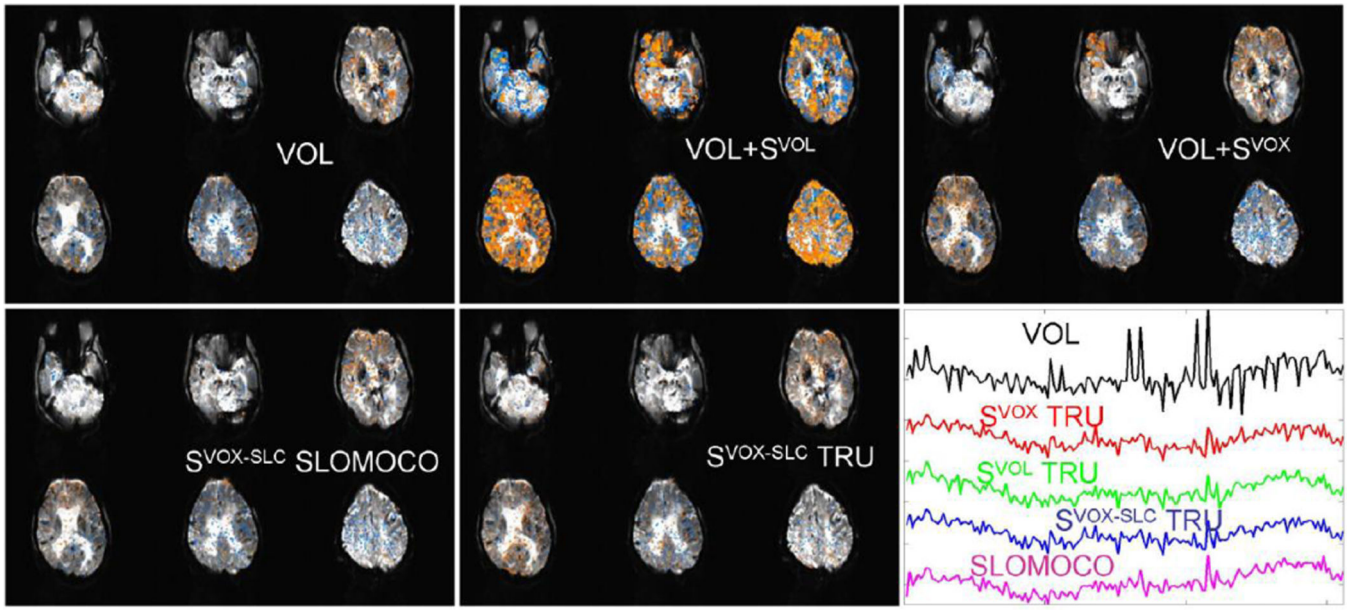

Fig. 7.

Performance of motion correction methods on rs-fMRI analyses in cadaver subject SimPACE data. Figure shows cadaver data corrected with VOL, VOL+ S^{VOL}, VOL+ S^{VOX}, $S^{VOX-SLC}$ with SLOMOCO and $S^{VOX-SLC}$ with TRU. Seed placed in posterior cingulate, each map shows InstaCorr connectivity at 0.4 correlation threshold. Timeseries plot in lower right shows selected voxel timeseries after each correction, showing the reduction in motion artifact with various motion models. Lower right corner shows same voxel location timeseries after each correction. Note the reduction in signal spikes at arbitrary motion injection timepoints every fourth volume during bulk of scan, as shown in Figure 2a.

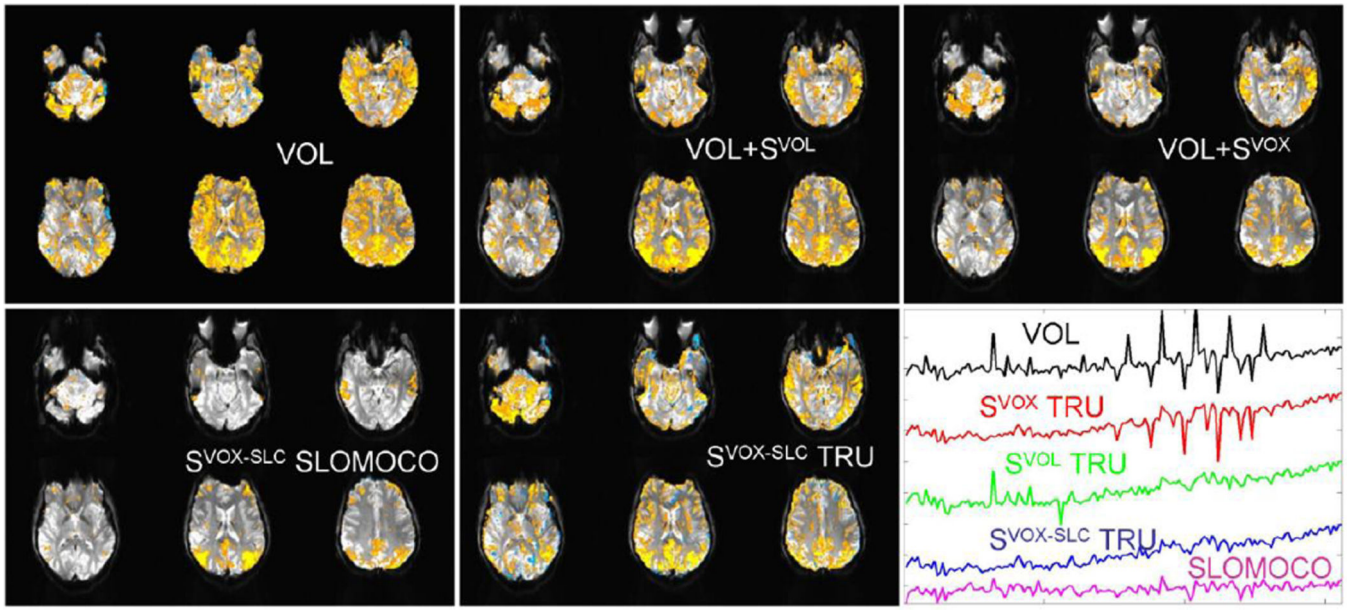

Fig. 8.

Performance of motion correction methods on rs-fMRI analyses in live subject SimPACE data. Figure shows subject data corrected for physiologic noise, then in parallel with VOL, VOL+ S^{VOL} TRU, VOL+ S^{VOX} TRU, $S^{VOX\text{-}SLC}$ with SLOMOCO and $S^{VOX\text{-}SLC}$ with TRU. Seed placed in posterior cingulate, each map shows InstaCorr connectivity at 0.4 correlation threshold. Timeseries plot in lower right shows selected voxel timeseries after each correction, showing the reduction in motion artifact with various motion models. Note the visual improvement of SLOMOCO retrospective correction over the best correction using the truth motion parameters ($S^{VOX\text{-}SLC}$ TRU), possibly due to real subject motion that differs from the injected motion. Lower right corner shows same voxel location timeseries after each correction. Note the reduction in signal spikes at arbitrary motion injection timepoints.

Table 1

Percent of corrupted volumes in SimPACE cadaver data identified by motion metrics. Motion was injected on 24% of volumes (12 out of 50 volumes). % corrupted indicates how many volumes were over the threshold. VTD and all BOLD signal-based metrics suffer from high false positive rates and reduced sensitivity compared to TD and FD. As noted in the text, none of the commonly used volumetric or signal-based motion metrics perform well.

	% Corrupted	TPR	FPR
Global signal-based metrics			
GS	58	75	53
PGS	0	0	0
VARS (0.5)	0	0	0
DVARS (0.5)	0	0	0
VARS (0.1)	2	8	0
DVARS (0.1)	8	17	5
Volumetric motion parameter-based metrics			
TD-0D	2	8.3	0
TD-1D	0	0	0
FD-0D	0	0	0
FD-1D	0	0	0
VTD-0D	24	66.7	10.5
VTD-1D	42	83.3	28.9
Idealized truth-based metrics (TRU)			
TD-0D-TRU	24	100	0
TD-1D-TRU	48	100	31.6
FD-0D-TRU	48	100	31.6
FD-1D-TRU	50	100	34.2
VTD-0D-TRU	38	75	26.3
VTD-1D-TRU	66	91.7	57.9

TPR=true positive rate; FPR=false positive rate.

Table 2

Accuracy of detected motion parameters with 3 volumetric coregistration tools. Accuracy assessed with linear Pearson correlation between volume-averaged injected motion and detected motion parameters across 6 DOF in 7 SimPACE cadaver datasets only

	Pearson linear correlation between injected and detected motion			
DOF	**AFNI**	**FSL**	**SPM**	**SLOMOCO (volavg)**
x-translation	0.8607 ± 0.2344	0.8793 ± 0.2274	0.9023 ± 0.1784	0.9004 ± 0.1723
y-translation	0.8241 ± 0.2417	0.8319 ± 0.2325	0.8652 ± 0.1945	0.8536 ± 0.1999
z-translation	0.9921 ± 0.004	0.9874 ± 0.0053	0.9877 ± 0.0051	0.9872 ± 0.0066
x-rotation	0.9679 ± 0.0119	0.9681 ± 0.0116	0.9912 ± 0.0057	0.9896 ± 0.0035
y-rotation	0.9726 ± 0.0103	0.9558 ± 0.0175	0.9909 ± 0.0066	0.9916 ± 0.0047
z-rotation	0.9932 ± 0.0061	0.9791 ± 0.0338	0.994 ± 0.0068	0.9897 ± 0.0105

DOF=degree of freedom.

Table 3

NMSE between the injected and detected parameters shown in Table 2

	NMSE between injected and detected motion		
DOF	**AFNI**	**FSL**	**SPM**
x-translation	0.3473 ± 0.176	0.2905 ± 0.1408	0.2649 ± 0.1342
y-translation	0.4443 ± 0.1821	0.4274 ± 0.1560	0.3705 ± 0.1374
z-translation	0.136 ± 0.037	0.1586 ± 0.0318	0.1627 ± 0.032
x-rotation	0.2718 ± 0.0402	0.2888 ± 0.0458	0.146 ± 0.0566
y-rotation	0.2525 ± 0.0282	0.3832 ± 0.0649	0.1395 ± 0.0491
z-rotation	0.1602 ± 0.0765	0.1588 ± 0.0504	0.1266 ± 0.0637

NMSE=normalized mean square error.

Table 4

Accuracy of SLOMOCO motion parameters compared with injected motion, averaged by volume and for every slice timepoint (number of slices × number of volumes). Third column is also shown in Table 2. Note that correlation to all slice timepoints is lower, but the number of timepoints is much greater.

	Averaged by volume - 156 timepoints		All slice timepoints - 4836 timepoints	
DOF	**All subjects (incl live subjects)**	**Cadavers only (7)**	**All subjects (incl live subjects)**	**Cadavers only (7)**
x-translation	0.7524 ± 0.3072	0.9004 ± 0.1723	0.5943 ± 0.2325	0.7019 ± 0.1541
y-translation	0.7128 ± 0.302	0.8536 ± 0.1999	0.6001 ± 0.2202	0.7043 ± 0.147
z-translation	0.9291 ± 0.1066	0.9872 ± 0.0066	0.8395 ± 0.0513	0.8641 ± 0.0172
x-rotation	0.9218 ± 0.1283	0.9896 ± 0.0035	0.7731 ± 0.0615	0.7969 ± 0.0306
y-rotation	0.9845 ± 0.0175	0.9916 ± 0.0047	0.7847 ± 0.0408	0.7795 ± 0.0466
z-rotation	0.8615 ± 0.2854	0.9897 ± 0.0105	0.7151 ± 0.1773	0.7977 ± 0.0786

Table 5

Mean tSTD for SimPACE motion injection data after various retrospective motion corrections, including volumetric correction with AFNI (VOL), second-order motion correction with VOL parameters ($\mathbf{S^{VOL}}$ and $\mathbf{S^{VOX}}$) and same after both VOL and second-order correction, and second-order correction with SLOMOCO ($\mathbf{S^{VOX\text{-}SLC}}$). SimPACE data separated into cadavers only and live subjects only. Bottom row shows ideal tSTD in cadavers in motion-free data (separate datasets acquired without motion-injection) and heavily scrubbed/censored data in the live subjects (81 timepoints removed out of 156 total).

Mean tSTD	**Data (cadavers only)**	**Data (live subjects only)**
Raw	41.53 ± 6.73	35.87 ± 3.54
VOL	30.13 ± 4.70	27.11 ± 1.62
$\mathbf{S^{VOL}}$	25.30 ± 3.65	22.63 ± 2.32
$\mathbf{S^{VOX}}$	21.16 ± 3.18	20.26 ± 2.05
VOL+$\mathbf{S^{VOL}}$	24.59 ± 3.27	20.93 ± 1.93
VOL+$\mathbf{S^{VOX}}$	20.13 ± 2.75	18.82 ± 1.69
$\mathbf{S^{VOX\text{-}SLC}}$ SLOMOCO	18.20 ± 2.6	17.86 ± 1.56
Motion-Free Raw	**10.01** ± **1.37**	22.04 ± 6.37

VOL=volumetric registration correction, S^{VOL}=second order motion regression with volumetric model, S^{VOX}=regression with voxel-specific model, $S^{VOX\text{-}SLC}$=second order motion regression with SLOMOCO algorithm.

Table 6

Mean tSTD for partial volume synthetic datasets and SimPACE motion injection data after several motion correction methods using, including regression of the gold-standard known injected motion (TRU), TRU averaged over each volume (TRU-AVG), and the TRU motion in the slicewise modified model ($\mathbf{S^{VOX\text{-}SLC}}$).

Mean tSTD	Cadaver Data	Live Subjects
Raw	41.53 ± 6.73	35.87 ± 3.54
$\mathbf{S^{VOL}}$ TRU-AVG	25.11 ± 3.47	24.90 ± 5.14
$\mathbf{S^{VOX}}$ TRU-AVG	21.48 ± 3.46	23.47 ± 4.92
$\mathbf{S^{VOX\text{-}SLC}}$ TRU-AVG	20.76 ± 3.44	22.79 ± 5.26
$\mathbf{S^{VOX}}$ TRU-SLC	18.83 ± 3.44	22.87 ± 5.16
$\mathbf{S^{VOX\text{-}SLC}}$ TRU-SLC	18.11 ± 3.24	22.18 ± 5.54

S^{VOL}=volumetric second-order motion regression, S^{VOX}=voxel-specific, volumetric second-order motion regression, $S^{VOX\text{-}SLC}$=voxel-specific, slicewise second-order motion regression, TRU=gold-standard truth injected motion, TRU-AVG=volume-averaged TRU, TRU-SLC= volume-maximal TRU motion.